Spectroscopic and Computational Studies of Spin States of Iron(IV) Nitrido and Imido Complexes

Lukas Bucinsky,[€] Martin Breza,[€] Wei-Tsung Lee,[†,‡,▼] Anne K. Hickey,[†] Diane A. Dickie,[§,⊥] Ismael Nieto,[‡] Jordan A. DeGayner,[☺] T. David Harris,[☺] Karsten Meyer,[‖] J. Krzystek,[$] Andrew Ozarowski,[$] Joscha Nehrkorn,[◊,●] Alexander Schnegg,[∂] Karsten Holldack,[∞] Rolfe H. Herber,[¶] Joshua Telser,[⊥,] and Jeremy M. Smith[†,‡,*]*

[€]Institute of Physical Chemistry and Chemical Physics, Faculty of Chemical and Food Technology, Slovak University of Technology, Radlinského 9, SK-81237 Bratislava, Slovakia.

[†] Department of Chemistry, Indiana University, 800 E. Kirkwood Ave., Bloomington, Indiana 47401, United States.

[‡] Department of Chemistry and Biochemistry, New Mexico State University, Las Cruces NM 88003, United States.

[§] Department of Chemistry and Chemical Biology, The University of New Mexico, Albuquerque, New Mexico 87131, United States.

[☺] Department of Chemistry, Northwestern University, Evanston, Illinois 60208, United States.

[‖] Department of Chemistry and Pharmacy, Friedrich-Alexander-University Erlangen-Nürnberg (FAU), Egerlandstraße 1, D-91058 Erlangen, Germany.

[$]National High Magnetic Field Laboratory, Florida State University, Tallahassee, Florida 32310, United States.

[◊] Department of Chemistry, University of Washington, Seattle, Washington 98195, United States.

[∂] Berlin Joint EPR Lab, Institute for Nanospectroscopy , Helmholtz-Zentrum Berlin für Materialien und Energie, Kekuléstraße 5, D-12489 Berlin, Germany

∞ Institut für Methoden und Instrumentierung der Forschung mit Synchrotronstrahlung, Helmholtz-Zentrum für Materialien und Energie, D-12489 Berlin, Germany

¶ Racah Institute of Physics, The Hebrew University of Jerusalem, 91904 Jerusalem, Israel.

| Department of Biological, Chemical and Physical Sciences, Roosevelt University, Chicago, Illinois 60605 United States.

▼ Current Address: Department of Chemistry and Biochemistry, Loyola University Chicago, Chicago, Illinois 60660, United States.

⊥ Current Address: Department of Chemistry, Brandeis University, Waltham, Massachusetts 02453, United States.

● Current Address: Department of Inorganic and Applied Chemistry, University of Hamburg, Hamburg, Germany

ABSTRACT

High-oxidation state metal complexes with multiply bonded ligands are of great interest for both their reactivity as well as their fundamental bonding properties. This paper reports a combined spectroscopic and theoretical investigation into the effect of the apical multiply bonded ligand on the spin state preferences of three-fold symmetric iron(IV) complexes with tris(carbene) donor ligands. Specifically, singlet ($S = 0$) nitrido [{PhB(Im^R)$_3$}FeN], R = ^{t}Bu (**1**), Mes (mesityl, **2**) and the related triplet ($S = 1$) imido complexes, [{PhB(Im^R)$_3$}Fe(NR′)]$^+$, R = Mes, R′ = Ad (1-adamantyl, **3**), ^{t}Bu (**4**), have been investigated by electronic absorption and Mössbauer effect spectroscopies. For comparison, two other Fe(IV) nitrido complexes, [($TIMEN^{Ar}$)FeN]$^+$, ($TIMEN^{Ar}$ = ***t***ris[2-(3-aryl-***im***idazol-2-ylidene)***e***thyl]ami***n***e; Ar = Xyl (xylyl), Mes), have been investigated by ^{57}Fe Mössbauer spectroscopy, including applied-field measurements. The paramagnetic imido complexes **3** and **4** were also studied by magnetic susceptibility measurements (for **3**) and paramagnetic resonance spectroscopy: high-frequency and -field electron paramagnetic resonance (HFEPR) (for **3** and **4**) and frequency-domain Fourier-transform (FD-FT) THz EPR (for **3**), which reveal their zero-field splitting (zfs) parameters. Experimentally correlated theoretical studies comprising ligand-field theory (LFT) and quantum chemical theory (QCT), the latter including both density functional theory (DFT) and *ab initio* methods reveal the key role played by the Fe $3d_{z^2}$ (a_1) orbital in these systems: the nature of its interaction with the nitrido or imido ligand dictates the spin state preference of the complex. The ability to tune the spin state through the energy and nature of a *single orbital* has general relevance to the factors controlling spin states in complexes with applicability as single molecule devices.

Introduction

The properties of transition metal imido and nitrido complexes have attracted interest in light of their relevance to dinitrogen functionalization,[1, 2] with iron complexes being of particular interest in the context of proposed mechanisms for ammonia synthesis by the Haber-Bosch process[3] and the nitrogenase enzyme.[4] It is therefore remarkable that as recently as 2000, there were no examples of isolable complexes containing iron-nitrogen multiple bonds, whether as imido $[Fe^{III,IV}{\equiv}NR]^{+,2+}$ or nitrido $[Fe^{IV,V}{\equiv}N{:}]^{+,2+}$ species. Indeed, these species were considered to be inherently unstable intermediates that would quickly rearrange or decompose in the absence of a substrate.[5] For example, Fe(IV) imido intermediates have been proposed in the formation of stable Fe(III) amido complexes.[6] This state of affairs changed with the isolation and crystallographic characterization of a stable iron imido complex,[7] which was, however, part of a multi-Fe cluster. Since then, structurally characterized mononuclear iron imido complexes have been reported for multiple geometries, oxidation states and spin states,[1, 8-15] extending to thermally stable and isolable iron bis(imido) complexes.[16-18]

By far the largest class of isolable iron imido complexes is that for which the supporting ligand creates a four-coordinate environment in approximate three-fold symmetry. Such ligands, often based on tris(phosphine) donors, have allowed for the synthesis of imido complexes in Fe(II),[19, 20] Fe(III),[21-27] Fe(IV)[27] oxidation states. Correspondingly, some of these supporting ligands likewise stabilize terminal iron nitrido complexes,[5, 28] such as the tris(phosphines)[29-31] tris(carbene)amine,[32] and tris(carbene)borate ligands.[33-35]

It is interesting to note that while all known examples of isolable Fe(IV) nitrido complexes are four-coordinate diamagnetic complexes with a three-fold symmetric iron center, analogous imido complexes show a greater structural diversity. For example, a tripodal

supporting ligand that contains a diphosphine and pyrazolyl mixed donor set has allowed for the isolation of a paramagnetic (S = 1) Fe(IV) imido complex,[27] while a pincer ligand has been shown to stabilize a diamagnetic (S = 0) Fe(IV) imido complex in a *cis*-divacant octahedral geometry.[36] Lastly, a recently reported,[37] four-coordinate, dipyrrinato formally Fe(IV) imido complex has been reinterpreted as high-spin Fe(III) anti-ferromagnetically coupled to an iminyl radical to give total spin, $S = 5/2 - 1/2 = 2$.[38]

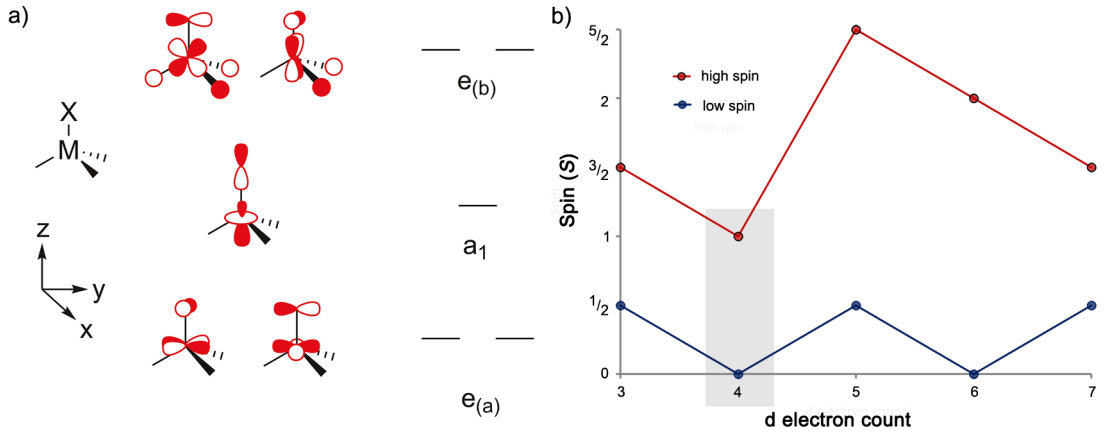

Figure 1. (a) Qualitative MO diagram for four-coordinate, three-fold symmetric complexes with scorpionate ligands. The relative energy of the a_1 orbital is variable; (b) High and low spin configurations in this geometry. Multiple spin states that have been experimentally observed for d^4 – d^7 electron configurations are indicated. Note that the low spin state (blue line; high spin is given by red line) is always the lowest possible spin state for the given electron configuration. The d^4 electron count is that studied here and is therefore highlighted.

N-Heterocyclic carbenes (NHCs) have recently become widely exploited as ligands to transition metal ions.[39, 40] Among the general class of NHC-donor ligands, bulky tris(carbene)borates[2, 40] are part of a larger class of scorpionate ligands that stabilize four-coordinate metal centers in three-fold symmetry.[41, 42] Since the discovery that bulky tris(pyrazolyl)borate ligands can stabilize this geometry,[43, 44] multiple complexes with different

d-electron counts have been reported. The resulting ligand field created by these rigid tripodal ligands creates opportunities for variation in electronic ground state configuration for a variety of d-electron counts (Figure 1), including spin-crossover behavior, i.e., two spin ground states within the same complex. While it might have been anticipated that the low coordination number would result in only high spin states, in practice complexes have been reported in multiple spin states for d^{4-7} electron counts. For higher d-electron counts, low spin states have been observed for complexes having both strongly donating scorpionate ligands and apical ligands that are strong π-donors, as exemplified by d^7 complexes where both high (S = 3/2, e.g., $Tp^{Me,iPr}CoI$)[45] and low (S = 1/2, e.g., BP_3CoI)[46, 47] spin states have been observed.[48] With the appropriate apical ligand, spin crossover has been observed for both iron[49, 50] and cobalt[51] complexes in which the scorpionate ligand contains strong field phosphine or NHC donors.[8, 49-54] Such tris(carbene) ligands are also notable in their ability to stabilize Fe(IV) imido[34] and nitrido[26, 32, 35] complexes in three-fold symmetry (Figure 1). The reactivity of the diamagnetic nitrido complexes has been extensively investigated, revealing one- and two-electron nitrogen atom transfer reactions with a range of substrates,[26, 27, 55, 56] including unsaturated hydrocarbons[57, 58] and low valent metal complexes.[59] While the reactivity of the Fe(IV) imido complex has been less extensively investigated, it is notable that the complex is paramagnetic (S = 1), in contrast to the nitrido complexes.

In this paper we build on this earlier work to understand the spin state preferences of four-coordinate complexes in three-fold symmetry having a d^4 electron configuration. Specifically, four-coordinate iron(IV) tris(carbene)borate complexes are observed for both S = 1 and S = 0 spin states (Figure 2), but the dependence of the spin state on the apical ligand (nitrido or imido) is not obvious. Since the $e_{(b)}$ orbitals are unoccupied for this d-electron count, the spin

state preference is not expected to depend directly on the nature of the tripodal ligand, in contrast to the d^6 and d^7 complexes described above.[60,61] Since the geometry imposed by the rigid scorpionate ligand leads to different spin state preferences for d^4 complexes than for isoelectronic octahedral complexes, where the $S = 1$ and $S = 2$ complexes are formed, we anticipate that insight into the factors dictating spin state preferences will be important for the design of magnetic molecules including applications such as spintronics[62] and in devices based on spin-crossover behavior.[63]

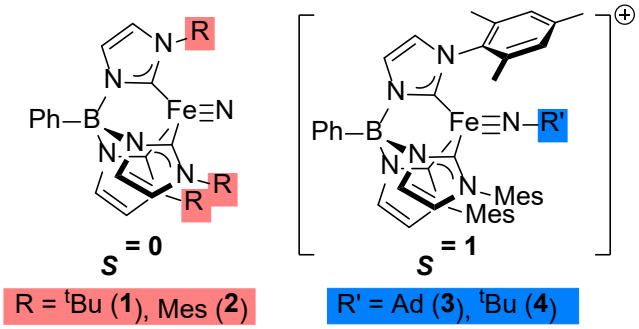

Figure 2. Iron(IV) nitrido (left) and imido (right) complexes supported by tris(carbene)borate ligands. In the nitrido complex, both R = *tert*-butyl (^{t}Bu, **1**) and mesityl (Mes, **2**) were investigated; for the imido complex, only R = Mes was studied, but with R′ = adamantyl (Ad, **3**) and *tert*-butyl (^{t}Bu, **4**).

We have applied a suite of experimental techniques to several iron(IV) nitrido ($[\{PhB(Im^R)_3\}FeN]^0$ and $[TIMEN^RFeN]^+$ (see Figures 2 and 3, respectively)[64] and imido complexes ($[\{PhB(Im^R)_3\}FeNR']^+$; see Figure 2, right) in combination with classical ligand-field theory (LFT) and advanced quantum chemical theory (QCT) calculations using both density functional theory (DFT) and *ab initio* methods to address this issue. The spectroscopic methods include temperature- and field-dependent ^{57}Fe Mössbauer measurements on nitrido and imido complexes. The paramagnetic tris(carbene) imido complexes have also been probed by magnetic resonance techniques, both in the field domain, using high-frequency and -field electron

paramagnetic resonance (HFEPR),[65, 66] and in the energy domain, using Fourier-transform frequency-domain terahertz EPR (FD-FT THz EPR) spectroscopy.[67-69] Magnetic susceptibility measurements have also been made of one of the imido complexes. These techniques taken in conjunction provide a measure of the zero-field splitting (zfs) of these spin triplet complexes, which yields information on their electronic structure.

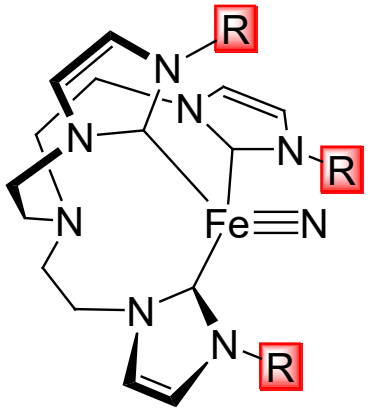

Figure 3. Iron(IV) nitrido complex supported by tris(carbene)amine ligands, denoted as $[(TIMEN^{R})FeN]^{+}$, where R = aryl = xylyl (Xyl) or mesityl (Mes).

In concert with the experimental studies listed above, we have also performed state-of-art computations on these three-fold symmetric Fe(IV) nitrido and imido complexes to provide theoretical insight into their electronic structure in general and spin state variability in particular. These studies have a broader relevance since, in striking contrast to the extensive theoretical studies on Fe(IV) oxido complexes, by Shaik, Que, and others,[70-74] there has not been the same depth of theory applied to the nitrogen-containing congeners. A limited number of studies have made theoretical comparisons between the reactivity of iron(IV) oxido and imido, as well as iron oxido and nitrido ligands have been made for four-fold symmetric complexes.[75-77] A valuable theoretical finding with respect to iron imido complexes has been made by Tangen et al.[52] who studied, among other topics, the effect of the bulky R substituents used in tris(phosphine)borate complexes on the Fe≡N-R′ geometry. Specifically, they found the Fe≡N-C′ angle to be bent in

the absence of the bulky R substituents on the tris(phosphine)borate ligand.[52] This work therefore will help to provide a more complete picture of iron(IV) complexes with multiply bonded ligands, and by extension, to similar complexes of other transition metal ions.

Experimental

Synthetic and crystallographic procedures

Complexes **1** and **2** were prepared according to literature procedures.[33-35] Crystals of the acetonitrile solvate **1·MeCN** ($C_{27}H_{38}BFeN_7 \cdot CH_3CN$) were grown from acetonitrile solution at −35 °C, as previously reported.[33] Solvent-free single crystals of the complexes (**1** and **2)** suitable for X-ray diffraction were grown from concentrated toluene solutions at room temperature. Complexes **3** and **4** were prepared as described previously for **3**,[26] with some modification, such as use of $^{t}BuN_3$ as the imido source for **4**. Further details are provided in the Supporting Information. The complexes [(TIMEN^{Ar})FeN](BPh$_4$), Ar = Mes, Xyl, were prepared as described previously.[32]

Mössbauer effect spectroscopy

Zero-applied field ^{57}Fe Mössbauer spectra of different compounds were recorded at multiple institutions: Hebrew University, Jerusalem, Israel (HU-J); Friedrich-Alexander University Erlangen-Nürnberg (FAU), Germany; Max-Planck-Institute for Chemical Energy Conversion (MPI CEC), Mülheim/Ruhr, Germany; and Indiana University, Bloomington, IN, USA (IU-B). In all cases, the isomer shifts are reported relative to the centroid of the spectrum of α-Fe at 298 K. Zero-field ^{57}Fe Mössbauer spectra at FAU-Erlangen were recorded on a WissEl Mössbauer spectrometer (MRG-500) at 78 K in constant acceleration mode using ^{57}Co(Rh) at room temperature as the radiation source. The temperature of the samples was controlled by an MBBC-HE0106 MÖSSBAUER He/N_2 cryostat within an accuracy of ±0.3 K. A similar

procedure was used at HU-J.[78] The experimental samples were shipped in sealed ampoules and transferred in an inert atmosphere glovebox to O-ring sealed Perspex sample holders which were immediately cooled to liquid nitrogen temperature and mounted cold in the cryostat. The temperature dependence of the Mössbauer spectra for several of these complexes was also analyzed to provide information on atomic vibrations[78-86] as described in Supporting Information. Mössbauer spectra of **3** were recorded at IU-B on a SEE Co spectrometer. The sample temperature (4.5 K) was controlled using a SVT-400 Dewar from Janis equipped with a Lake Shore 255 Temperature Controller. Data analysis was performed using the program WMOSS.[87]

Applied-field ^{57}Fe Mössbauer spectra of several nitrido complexes were recorded at MPI CEC on a conventional spectrometer with alternating constant acceleration of the γ-source. The sample temperature was maintained constant in an Oxford Instruments Mössbauer-Spectromag cryostat, which is a split-pair superconducting magnet system for applied fields up to 8 T where the temperature of the sample can be varied in the range 1.5 K to 250 K. The field at the sample is perpendicular to the γ-beam. The ^{57}Co/Rh source (1.8 GBq) was positioned at room temperature inside the gap of the magnet system at a zero-field position, by using a re-entrant bore tube. WinNormos for Igor Pro software was used for the quantitative evaluation of the spectral parameters (least-squares fitting to Lorentzian peaks). The minimum experimental line widths in cases were maximally 0.24 mm s^{-1} (full width at half-height, fwhm). Magnetic Mössbauer spectra were simulated with the spin Hamiltonian program MX (by E. Bill) by diagonalization of the usual nuclear Hamiltonians for ground and excited states of ^{57}Fe.[88] The electron spin was $S = 0$ throughout.

HFEPR spectroscopy

HFEPR spectra of powdered samples of **3** and **4** (each roughly 50-100 mg) were obtained using two separate spectrometers at the National High Magnetic Field Laboratory (NHMFL, Tallahassee, FL, USA). The one located within the Electron Magnetic Resonance (EMR) Facility used a 15 T superconducting magnet and is identical to that described previously,[89] with the exception of employing a Virginia Diodes (Charlottesville, VA, USA) source operating at a base frequency of 12 – 14 GHz and multiplied by a cascade of multipliers. Phase-sensitive detection was used, with the magnetic field modulated at 50 kHz, so that traditional, first-derivative mode spectra result. Low temperature control was provided by an Oxford Instruments (Oxford, UK) continuous flow cryostat. The spectrometer that is associated with the DC Field Facility uses a fast sweepable, resistive ("Keck") 25 T magnet and backward wave oscillator (BWO) sources, as described elsewhere.[90] An optical chopper provides modulation of the sub-THz wave beam so that the resulting spectra are in absorption mode. HFEPR spectra were recorded in the temperature range 4.2 – 10 K.

FT-FD THz-EPR spectroscopy

FD-EPR spectra were measured on the Frequency Domain Fourier Transform (FD-FT) THz EPR spectrometer at the electron storage ring BESSY II, which is described in more detail elsewhere.[68, 69] This setup employs broadband THz radiation emitted by a Hg arc lamp or, in the present case, a synchrotron for EPR excitation. The sample is contained within a superconducting magnet so that spectra at zero-field and at a series of external magnetic fields up to ±10 T can be recorded. A superfluid He cooled bolometer mounted at the end of the quasi-optical transmission line serves as the detector. A referencing procedure described in detail elsewhere was employed to properly identify absorption bands of interest.[67] Due to limitations on

material and beam-time, only complex **3** was studied by this technique. A powder sample of **3** (45 mg) was thoroughly mixed with polyethylene powder (106 mg) and pressed into a pellet. The experimental spectral resolution was 0.025 cm^{-1}, which corresponds to a minimum line width of 0.0425 cm^{-1}.

HFEPR spectra were simulated using the program SPIN (by A. Ozarowski), which employs a standard spin Hamiltonian for spin triplets:

$$\mathcal{H} = \beta_e B \cdot \boldsymbol{g} \cdot \hat{S} + D\left(\hat{S}_z^{\,2} - \frac{1}{3} S\left(S+1\right) \right) + E\left(\hat{S}_x^{\,2} - \hat{S}_y^{\,2} \right) \qquad (1)$$

FT-FD THz-EPR were simulated using the same spin Hamiltonian and with the programs EasySpin, from S. Stoll,[67, 91] and DDPOWHEA, from J. Telser. The HFEPR spectra were reasonably well reproduced using an ideal powder pattern model; however, the FT-FD THz spectra with external field did not exhibit the expected powder pattern and the deviation increased with field magnitude. This behavior has been seen previously.[67] We have therefore used a phenomenological model to reproduce the frequency domain spectra recorded with applied fields.

Magnetic Susceptibility

Magnetic data were collected using a Quantum Design MPMS-XL SQUID magnetometer for compound **3** as a finely ground microcrystalline powder sealed in a polyethylene bag under a dinitrogen atmosphere. Direct current (dc) magnetic susceptibility data were collected in the temperature range 1.8 – 300 K under an applied field of 1 T. All data were corrected for diamagnetic contributions from the sample holder and for core diamagnetism of **3** (estimated using Pascal's constants).[92] The data were fitted using a spin Hamiltonian for $S = 1$ (Eqn 1), but with only axial zero-field splitting terms (i.e., $E = 0$) and isotropic g. Two programs were used,

DSUSFITP from J. Telser and MagProp, which is part of the NIST DAVE neutron spectroscopy analysis software package.{Azuah, 2009 #65;Tregenna-Piggott, 2008 #66} The two programs gave essentially identical fit results.

Ligand-field theory

Calculations using the entire d^4 basis set were performed using the program Ligfield,[93] by J. Bendix, and the locally written programs DDN and DDNFIT, the latter of which allows fitting of experimental d-d electronic absorption bands to LFT parameters. Free-ion values for the spin-orbit coupling (SOC) parameter, ζ, and Racah inter-electronic repulsion parameters, *B* and *C*, were taken from those reported by Brorson, Bendix, and co-workers.[94, 95]

Quantum chemical theory

Geometry optimizations of compounds under study in singlet, triplet and/or quintet spin states were performed using the Gaussian® G09 program suite[96] employing the B3LYP/6-311G*[97-103] level of theory (starting from previously reported[26, 33, 34] and/or current experimental X-ray diffraction structures except for cation **4** which has been obtained from **3** by manually changing the adamantyl group to *tert*-butyl) without any symmetry restrictions. The optimizations included vibrational frequency analysis of the resulting energy minima to avoid transition state or saddle point geometries.

Relative energies of various spin states of the same complex have been corrected using restricted open-shell single-point calculations (replacing the electron energy in unrestricted energy data) except "broken symmetry" singlet state (BS) where the energy difference between singlet (E_S) and triplet (E_T) states is evaluated as given in Eqn 2:

$$E_S - E_T = \frac{\left(E_{BS} - E_{uT}\right)}{\left(1 - 0.5\left\langle S^2 \right\rangle_{BS}\right)} \qquad (2)$$

where E_{uT} is an open-shell energy of the triplet state, and E_{BS} and $\langle S^2 \rangle_{BS}$ are the energy and spin expectation values of the "broken symmetry" singlet state, respectively.[104, 105]

The zfs parameters,[106] **g** tensors,[107, 108] and Mössbauer parameters (isomer shifts and quadrupole splittings) were evaluated using the ORCA software package[109] assuming singlet spin states for **1** and **2** or triplet spin states for **3** and **4**. The UBLYP[97, 98]/TZVP[110] zfs parameters have been calculated with either the coupled perturbed (CP)[111] and/or quasi restricted orbital (QRO)[106] methods for comparison completeness. The B3LYP/TZVP/COSMO(water) (COSMO = COnductor-like Screening MOdel) Mössbauer isomer shifts (δ) have been estimated using the fitted trend line from Römelt et al.[112] The specific trend line used was for the optimized geometries obtained at TPSS functional[113] / TZVP basis set / COSMO(water)[114] solvent model level of theory. B3LYP/TZVP/COSMO(water) quadrupole nuclear moments have been calculated according to Neese and co-workers.[112, 115] Complete active space self-consistent field (CASSCF)[106, 116-118] results were based on an active space of 10 electrons in 8 orbitals (10,8), to account for the d-electrons of iron, including the σ and π interactions within the $[Fe{\equiv}N(R')]^{+(2+)}$ moiety. The *D* and *E* contributions are calculated based upon the state average formalism, using a reasonable number of configurations, i.e., 50 quintet, 100 triplet and 100 singlet states (for the state specific CASSCF wave function, see Results). State averaging of the nearly degenerate $3d_{xy}{}^1 d_{x^2-y^2}{}^2 d_{z^2}{}^1$ / $3d_{xy}{}^2 d_{x^2-y^2}{}^1 d_{z^2}{}^1$ configurations has been also taken into account at the CASSCF level of theory; denoted as sa-CASSCF.

The electronic structure of the complex under study has been explored at the B3LYP and state specific as well as state averaged CASSCF levels of theory. The electronic structure was elucidated via localized orbitals,[119] natural orbitals, and Mulliken population analysis of atomic d- and s-orbitals, as well as Quantum Theory of Atoms in Molecules (QTAIM) analysis.[120] A

brief description of the QTAIM analysis method with respect to electron density topology is given in Supporting Information. Atomic d- and s- populations are considered for a rotated geometry of the complex with the nitrido or imido ligand defining the *z*-axis direction and one equatorial carbene C atom defining the *xz* plane. QTAIM analysis was performed in the AIM2000 package[121] using the wave function from the G09 wfn file. Localized and natural orbitals were visualized in the Chemcraft software package[122] (color scheme: cyan, pink, yellow, violet, and silver for H, B, C, N, and Fe, respectively).

Results and Discussion

X-ray crystallography

While the iron(IV) nitrido complexes **1** and **2** had been previously reported, their X-ray crystal structures were obtained for solvated complexes, e.g., **1·MeCN**. We now report that crystallization from concentrated toluene solutions provides structures that are free of solvent (Figure 4). The relevant metrical parameters of these structures show slight differences in comparison to the previously reported structures (R = Mes, CSD code: QOXBOV[34]; R = ^{t}Bu, CSD code: JOGGOC;[33] see Table 1). Most notably, the Fe-N bond lengths are longer (by 0.02 and 0.01 Å for **1** and **2**, respectively) in the unsolvated structures. The shorter bonds in the solvated complexes might be attributed to nitrido ligand interactions with MeCN (e.g., Fe≡N···H-C closest contacts are 2.46 and 2.67 Å for **1·MeCN** and **2·MeCN**, respectively), however, this was not revealed computationally (see QCT section below), so that any differences are more likely due to crystal packing effects that cannot be quantified. Despite the slight elongation, the Fe-N bond lengths in **1** and **2** are still markedly shorter than in the previously reported iron(IV) imido complex **3** (CSD code: MOBNUN) where the Fe-N distance is 1.618(3) Å.[26] Note that the

corresponding distances in the Fe(IV) imido complexes [{PhB($CH_2P(^tBu)_2)_2(pz^{R,R})$}Fe(NAd)]($BAr^{F24}$), where BAr^{F24} = $B(3,5\text{-}(CF_3)_2C_6H_3)_4^-$, are 1.609 Å and 1.634 Å, respectively for R = H, Me,[27,123] thus giving an average (1.622 Å) very close to that of **3**.

The Fe-C bond lengths to the carbene donors are generally shorter for **2** than for **1**, which we attribute to the different topologies of the tris(carbene)borate ligands. Specifically, the flatter mesityl group provides a different steric impediment than the *tert*-butyl group, allowing for shorter metal-ligand bonds. The Fe-C bond lengths for all nitrido complexes are significantly shorter than in the one crystallographically characterized imido complex, **3**. Qualitatively, this is due to the Fe in the nitrido complexes being a stronger Lewis acid than in the imido complex, despite the imido complex being overall positively charged. The bonding aspects will be discussed quantitatively in the QCT section below.

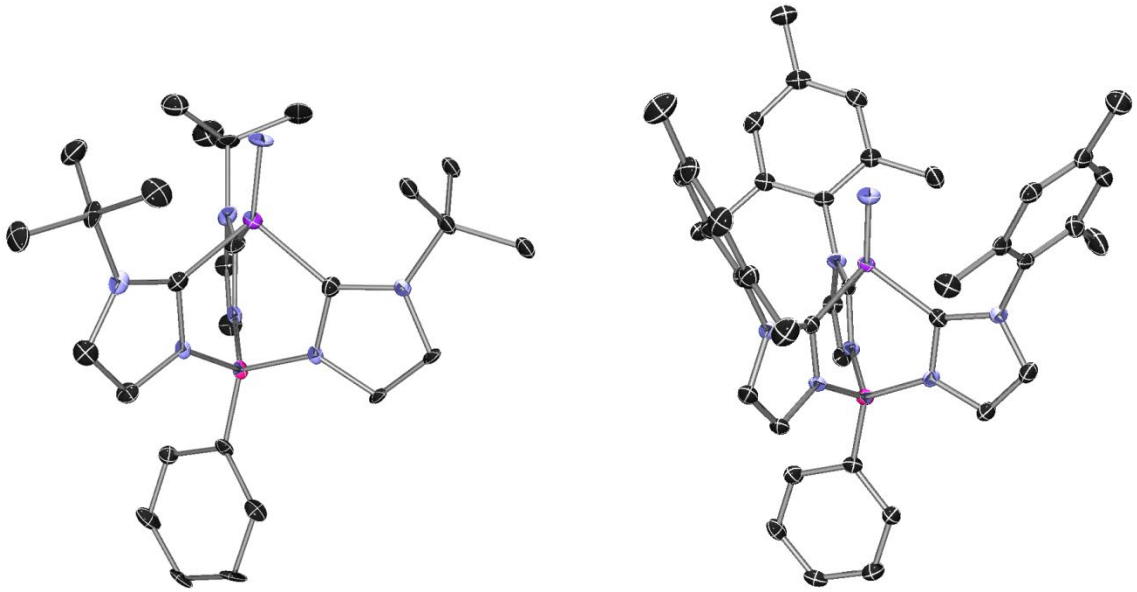

Figure 4. X-ray crystal structures of unsolvated iron(IV) nitrido complexes **1** and **2**. Thermal ellipsoids shown at 50 % probability, hydrogen atoms omitted for clarity. Black, blue, purple, and pink ellipsoids represent C, N, Fe, and B atoms, respectively.

Table 1. Selected distances (Å) and angles (°) crystallographically determined for the tris(carbene)borate iron(IV) nitrido and imido complexes under study.

Complex	(R = ^{t}Bu)		(R = Mes)		
	1	**1·MeCN** [a]	**2**	**2·MeCN** [b]	**3** [c]
Fe-N	1.532(5)	1.512(1)	1.509(2)	1.499(5)	1.618(3)
Fe-C	1.917(9)	1.915(1)	1.895(3)	1.885(7)	1.956(9)
	1.917(9)	1.928(1)	1.903(3)	1.916(6)	1.972(3)
	1.930(7)	1.928(1)	1.910(3)	1.921(6)	1.978(3)
N-Fe-C	120.1(3)	119.82(6)	121.5(1)	120.7(3)	123.2(1)
	120.7(3)	120.85(6)	122.0(10)	122.2(3)	125.8(1)
	121.6(3)	121.44(6)	122.5(1)	123.3(3)	128.3(1)

[a] CSD code: JOGGOC.[33]
[b] CSD code: QOXBOV.[34]
[c] R′ = Ad; CSD code MOBNUN.[26]

^{57}Fe Mössbauer spectroscopic measurements

The ^{57}Fe Mössbauer spectra of three-fold symmetric iron(IV) nitrido complexes previously reported are notable.[1, 2, 32] In addition to the negative isomer shift, (δ = –0.27 to –0.34 mm s^{-1}), they also display very large quadrupole splittings, (ΔE_Q = 5.99 to 6.23 mm s^{-1}) at 78 K. Indeed, the quadrupole splittings are among the largest ever measured,[124, 125] which is attributed to the highly anisotropic electron distribution, with all the 3d electrons confined to the *xy* plane (Figure 1).

We previously reported the Mössbauer spectrum of unsolvated **2** at 78 K.[126] Similarly to that complex, the zero-field Mössbauer spectra of both the solvated (**1·MeCN**; Figure 5, upper left) and unsolvated forms of **1** (not shown) give rise to well resolved doublets. The isomer shift (δ) and quadrupole splittings (ΔE_Q) of complexes **1·MeCN** and **2** are similar at 90 K, including

large quadrupolar interactions (Table 2). The Mössbauer parameters of **1** are somewhat different from those observed for **1·MeCN**, likely due to the slightly different bond metrics in this crystal structure as well as interactions with the crystallized solvent, as described above. Applied-field (7 T) Mössbauer spectra were also recorded for **1·MeCN (**Figure 5, lower left) and for the two nitrido complexes supported by TIMEN^{R} ligands (R = Mes (Figure 5, lower right) Xyl (Figure S4, Supporting Information). The zero-field and applied-field spectra give consistent isomer shifts and quadrupole splittings. The applied-field spectra determine the positive sign of the electric field gradient (EFG, ΔE_Q) and confirm the $\left(d_{x^2-y^2}, d_{xy}\right)^4$ electron configuration with its S = 0 spin ground state of the nitrido complexes. The applied-field spectra also reveal any rhombicity in the quadrupole coupling tensor. It is interesting to note that the two TIMEN^{R} complexes have rigorously axial quadrupole coupling ($\eta = 0$), as expected for trigonal symmetry, but there is slight rhombicity ($\eta = 0.1$; 1 is the maximum possible) in the tris(carbene)borate complex resulting from the chelate's phenyl borate anchor that removes the three-fold axial symmetry. This geometrical distortion may also be reflected in the Jahn-Teller effects that are manifest in the paramagnetic imido complexes **3** and **4**.

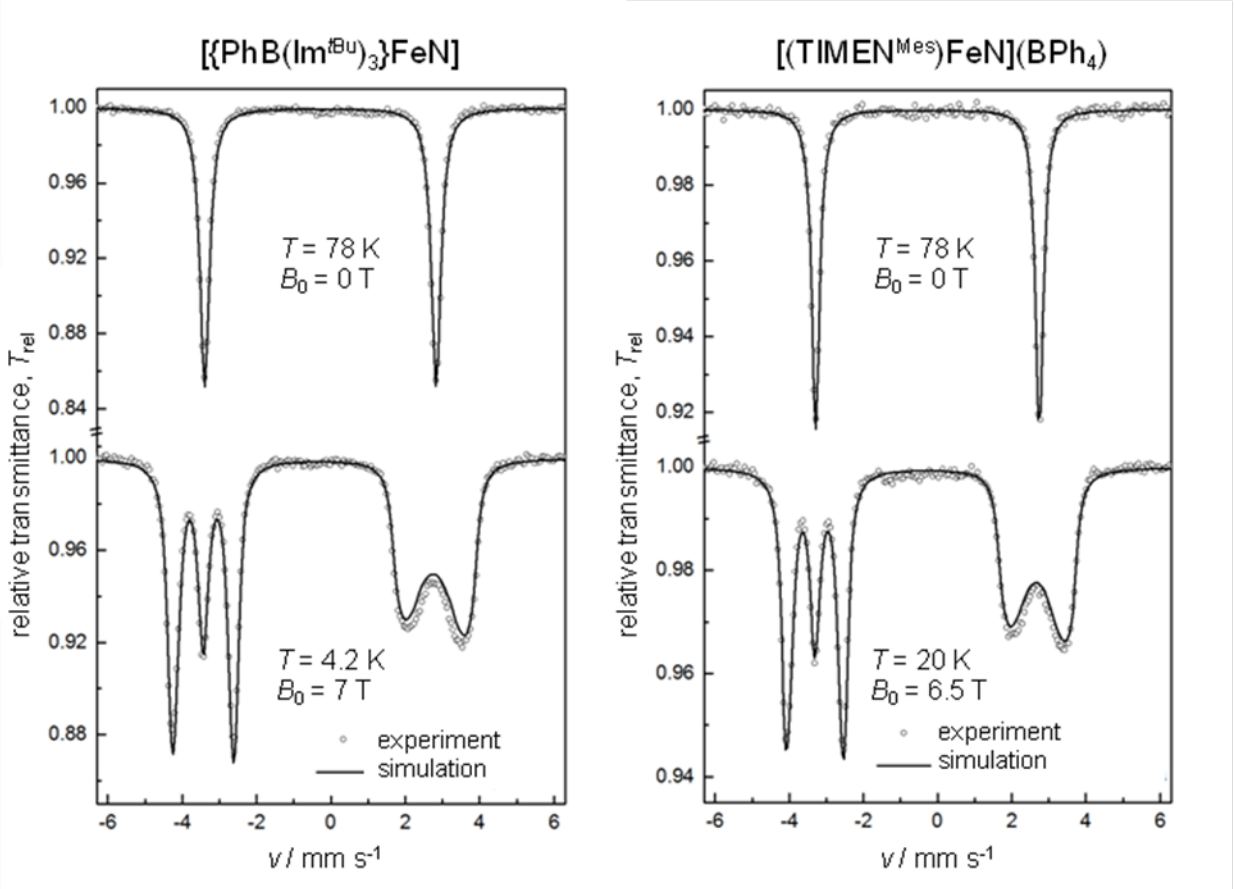

Figure 5. Zero-field (top) and magnetic-field applied (bottom) ^{57}Fe Mössbauer spectra of left: **1•MeCN**; right: [(TIMEN^{Mes})FeN](BPh$_4$). The zero-field spectra were recorded at 78 K; the spectra with a field applied perpendicular to the γ-rays were recorded at 7 T and 4.2 K for **1•MeCN** and at 6.5 T and 20 K for [(TIMEN^{Mes})FeN](BPh$_4$). The solid lines are powder simulations for S = 0, obtained with the parameters: δ = –0.31(1) mm s^{-1}, ΔE_Q = +6.21(1) mm s^{-1}, Γ_{fwhm} = 0.26(1) mm s^{-1}, η = 0.10 for **1•MeCN**; δ = –0.30(1) mm s^{-1}, ΔE_Q = +5.99(1) mm s^{-1}, Γ_{fwhm} = 0.26(1) mm s^{-1}, η = 0 for [(TIMEN^{Mes})FeN](BPh$_4$).

The zero-field Mössbauer spectrum of **3** is shown in Figure 6. Mössbauer spectra of **4** were not recorded due to limitations on material availability. Complex **3** exhibits a well-resolved doublet with a negative isomer shift similar to its nitrido analogs, but with a much smaller quadrupole splitting (Table 2). Unfortunately, it has not proven possible to prepare imido complexes of iron supported by the TIMEN^R ligand. Indeed, in contrast to the

[{PhB(Im^{R})$_3$}FeN] complexes, the nitrido ligand in [(TIMEN^{R})FeN]$^{+}$ complexes shows no reactivity. We speculate that this inertness is due to TIMEN^{R} forming a deep and narrow cavity that also greatly inhibits side-on access to the axial ligand.

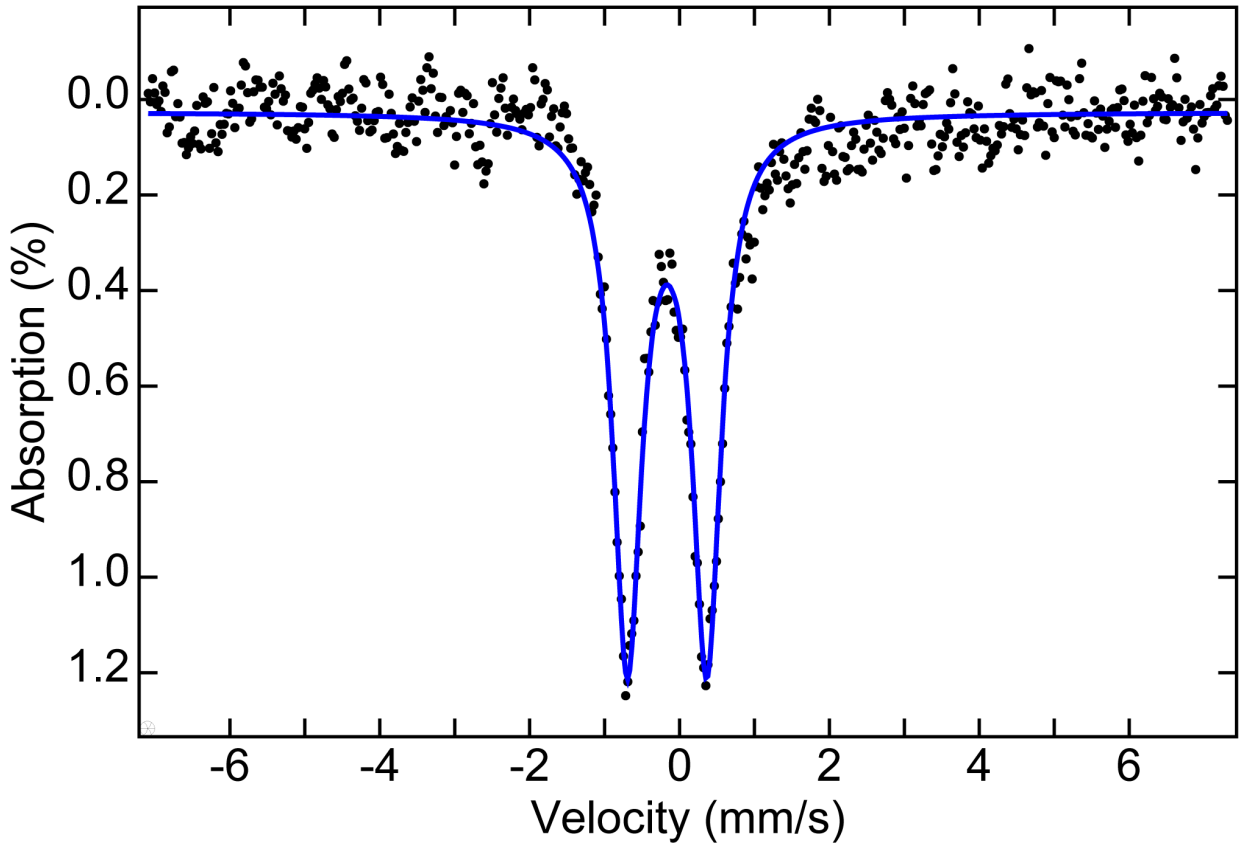

Figure 6. ^{57}Fe Mössbauer spectrum of **3** at 80 K. The blue trace is a simulation using δ = –0.17 mm s^{-1} and ΔE_Q = 1.06 mm s^{-1}.

Table 2. Experimental and computed Mössbauer spectral parameters for Fe(IV) nitrido and imido complexes.

Complex	*S*	Method (Geometry) [a]	δ (mm s^{-1})	ΔE_Q (mm s^{-1})	*T* (K)	Reference
Nitrido complexes						
1·MeCN	0	Experiment	–0.28(1)	6.23(1)	78	This work [k]
		Experiment	–0.31(1)	6.21(1)	4.2 [i]	This work
		B3LYP (exp)	–0.3245	5.436		This work
		B3LYP (exp [h])	–0.3165	5.436		This work
2·MeCN	0	Experiment	–0.28(1)	6.08(1)	78	This work
1	0	Experiment	–0.323(20)	6.18(6)	90	This work
		B3LYP (exp)	–0.2943	5.480		This work
		B3LYP (opt)	–0.3047	5.447		This work
2	0	Experiment	–0.354(6)	6.171(6)	90	This work
		B3LYP (exp)	–0.3202	5.362		This work
		B3LYP (opt)	–0.3157	5.416		This work
[(TIMEN^{Mes})FeN](BPh$_4$) [b]	0	Experiment	–0.30(1)	5.99(1)	20 [j]	This work
[(TIMEN^{Xyl})FeN](BPh$_4$) [b]	0	Experiment	–0.31(1)	5.97(1)	20 [j]	This work
Imido complexes						
3	1	Experiment	–0.17(1)	1.06(1)	80	This work
		B3LYP (exp)	–0.2155	1.464		This work
		B3LYP (opt)	–0.1417	1.451		This work
4	1	B3LYP (opt)	–0.1591	1.436		This work [l]
(pyrr$_2$py)Fe=NAd [c]	0	---	–0.09(1)	2.78(1)	77	[36]
Fe$_4$(μ$_3$-N^{t}Bu)$_4$(N^{t}Bu)Cl$_3$	[f]	---	–0.17(2)	0.38(3)	150	[7]
(^{tBu}L)FeCl(•NC$_6$H$_3$-2,6-iPr$_2$) [d]	2 [g]	---	+0.37	2.17	90	[38]
[Fe(NTs)(N4Py)]$^{2+}$ [e]	2	---	+0.02	+0.98	4.2	[127]

[a] Applies only to B3LYP calculations and the usage of either the experimental (exp) or optimized (opt) geometry.
[b] TIMEN^{R} = tris[2-(3-aryl-imidazol-2-ylidene)ethyl]amine, where R = aryl = xylyl (Xyl), mesityl (Mes).
[c] pyrr$_2$py = bis(pyrrolyl)pyridine dianion.
[d] ^{tBu}L = 1,9-di-*tert*-butyl-5-(2,6-dichlorophenyl)dipyrromethene anion.
[e] N4Py = *N*,*N*-bis(2-pyridylmethyl)bis(2-pyridyl)methylamine, Ts = tosyl; this complex was studied in solution and not isolated as a stable solid.
[f] Spin-coupled cluster, so the spin of individual Fe site is not well determined. The cluster has been described as valence localized Fe(III)$_3$Fe(IV), wherein the Fe(III) sites are likely high-spin.[7] We speculate that the net cluster spin S = 1/2 could arise from an anti-ferromagnetically coupled Fe(III)$_2$ pair (total S = 0) together with an anti-ferromagnetically coupled Fe(III)Fe(IV) pair (total S = 1/2). This coupling scheme is analogous to those proposed for $[Fe_4S_4]^{0,+,2+}$ clusters,[128] but does not give us the individual spin states within the Fe(III)Fe(IV) pair.
[g] Described as S = 5/2 Fe(III) antiferromagnetically coupled to S = 1/2 iminyl radical to give total spin S = 2.
[h] Calculation included the presence of the MeCN solvent molecule.
[i] Mössbauer spectra recorded with an external magnetic field of 7 T applied perpendicular to the incident γ rays. Analysis of these data gave η = 0.10 for the quadrupole coupling.
[j] Mössbauer spectra recorded both at zero-field (at 78 K) and with an external magnetic field of 6.5 T applied perpendicular to the incident γ rays. Parameters derived only from the applied-field data are given; these also gave η = 0.00 for the quadrupole coupling.
[k] Zero-field Mössbauer spectra for **1·MeCN** have also been previously reported.[35]
[l] Note that Mössbauer spectra were not recorded for **4**, but optimized geometry calculations were performed for comparison with experiment and calculations for **3**.

To the best of our knowledge, only two bona fide iron(IV) imido complexes have been previously characterized by Mössbauer spectroscopy (Table 2).[7, 36] Although these complexes have different geometries and spin states from **3**, their isomer shifts are similar to those of **3**, particularly that of the first example of an iron(IV) imido complex, $Fe_4(\mu_3\text{-}N^tBu)_4(N^tBu)Cl_3$,[7] where the imido ligand is bound to one iron atom of a spin-coupled paramagnetic iron cluster. The close similarity of these parameters suggest that the iron center in both complexes is in the same environment. In contrast, the dipyrrinato iron imido complex has an isomer shift distinctly different from those of the others, (i.e., positive; see Table 2) which observation contributes to its

description as S = 5/2 Fe(III) anti-ferromagnetically coupled to an S = 1/2 iminyl (Ar-N$^{\bullet-}$) radical.[38]

Magnetic susceptibility

The imido complex **3** was investigated by DC magnetic susceptibility, which is the most readily accessible technique for the investigation of zfs in complexes with $S > 1/2$.[129] The high temperature ($T \geq 90$ K) average value for the magnetic moment, $\mu_{eff} = 2.91$, corresponds to a spin-only value for $S = 1$ with $g = 2.06$, which is reasonable on its own as well as consistent with the magnetic resonance results (*vide infra*). At lower temperatures, the molar susceptibility (χ) decreases, indicative of zfs, as seen in a plot of χT versus T, Figure 7. Unfortunately, this qualitative picture was difficult to quantify. In order for the fitting process to match the high temperature region at all successfully, it was necessary to fix the (isotropic) g value at 2.06; the zfs was fixed as axial, as magnetic susceptibility is generally insensitive to rhombic zfs,[130, 131] and the magnetic Mössbauer and magnetic resonance results showed that the system is nearly axial. Oftentimes, magnetic susceptibility fits are insensitive to the sign of D, thus providing the same $|D|$ regardless of whether the fit is fixed negative or positive.[130, 131] However, in this case distinctly different results obtained for each of these cases, as shown in Figure 7. For positive D, the very low temperature ($T < 10$ K) data are relatively well fitted, while the intermediate temperature (10 K $\leq T <$ 80 K) data are relatively poorly fitted. In contrast, for negative D, the low T data are poorly fitted and the intermediate temperature data are well fitted. This would be of little consequence if the resulting $|D|$ values were similar, but they are not. For positive D, the best fit is +14.5(5) cm^{-1}, while for negative D, it is –33.7(5) cm^{-1}, independent of whether the isotropic g value is also allowed to vary or is fixed at the high temperature value, $g = 2.105$.

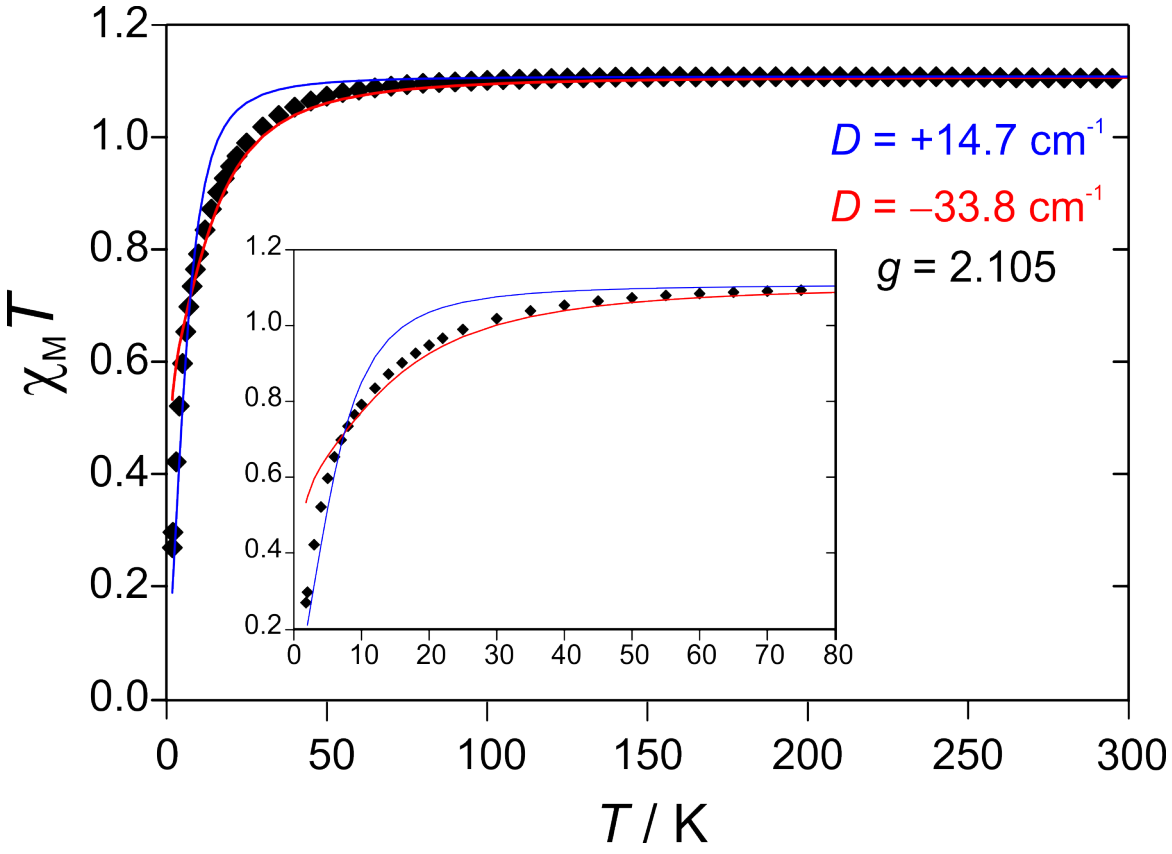

Figure 7. DC magnetic susceptibility of **3** plotted as molar $\chi_M T$ versus T. Data points are given by diamonds and were recorded at an applied field of 1 T. Fit lines using an $S = 1$ spin axial Hamiltonian are shown for both positive (blue traces) and negative (red traces) D values, as shown on the figure, with g_{iso} fixed at 2.105. The inset shows the lower temperature region where the differences between the fits are more evident.

HFEPR

By virtue of being a resonance technique, HFEPR is inherently more desirable to extract zfs parameters from an $S > 1/2$ system.[132] Both imido complexes **3** and **4** were therefore investigated as polycrystalline solids by HFEPR. For a spin triplet with relatively large zfs, the EPR transitions are few in number, as some of us have previously seen with tetragonal oxidoiron(IV) complexes.[133] Nevertheless, by observation of resonances at or near zero applied field, the zfs can be readily extracted. The field dependence of these resonances can be followed

at higher frequencies, which allows the *g* values to be determined – parameters that are not readily available from Mössbauer spectroscopy, even with applied fields.

Compound **4** gave a better HFEPR response and thus will be discussed first. Using the resistive magnet (Keck) setup, **4** unequivocally delivered two zero-field resonances, at frequencies of ca. 195 and ca. 208 GHz (Figure 8, lower panel). Both resonances could be followed to higher frequencies and higher fields, but nothing could be observed below 195 GHz, i.e., the complex is "EPR-silent" at that frequency range. At high enough frequency (ca. 300 GHz), the two transitions merged into a single line, observable until the end of the range of frequencies of the particular BWO source used, i.e., 360 GHz. No resonances could be detected using higher-frequency BWO sources, as these have lower power. The superconducting magnet-based spectrometer confirmed these results; however, the increased resolution of the derivative shape (due to magnetic field modulation and phase detection) resulted in an appearance of a structure on top of the broad resonances (see Figure S4, Supporting Information). Although in principle such structure in the main transition could originate from differing g_x and g_y values, this should result in the splitting increasing with frequency/field, yet it does not, remaining approximately constant. We believe that this behavior is an orientation artifact (i.e., from an imperfectly random ensemble of molecules) revealed by the increased resolution of the derivative spectra.

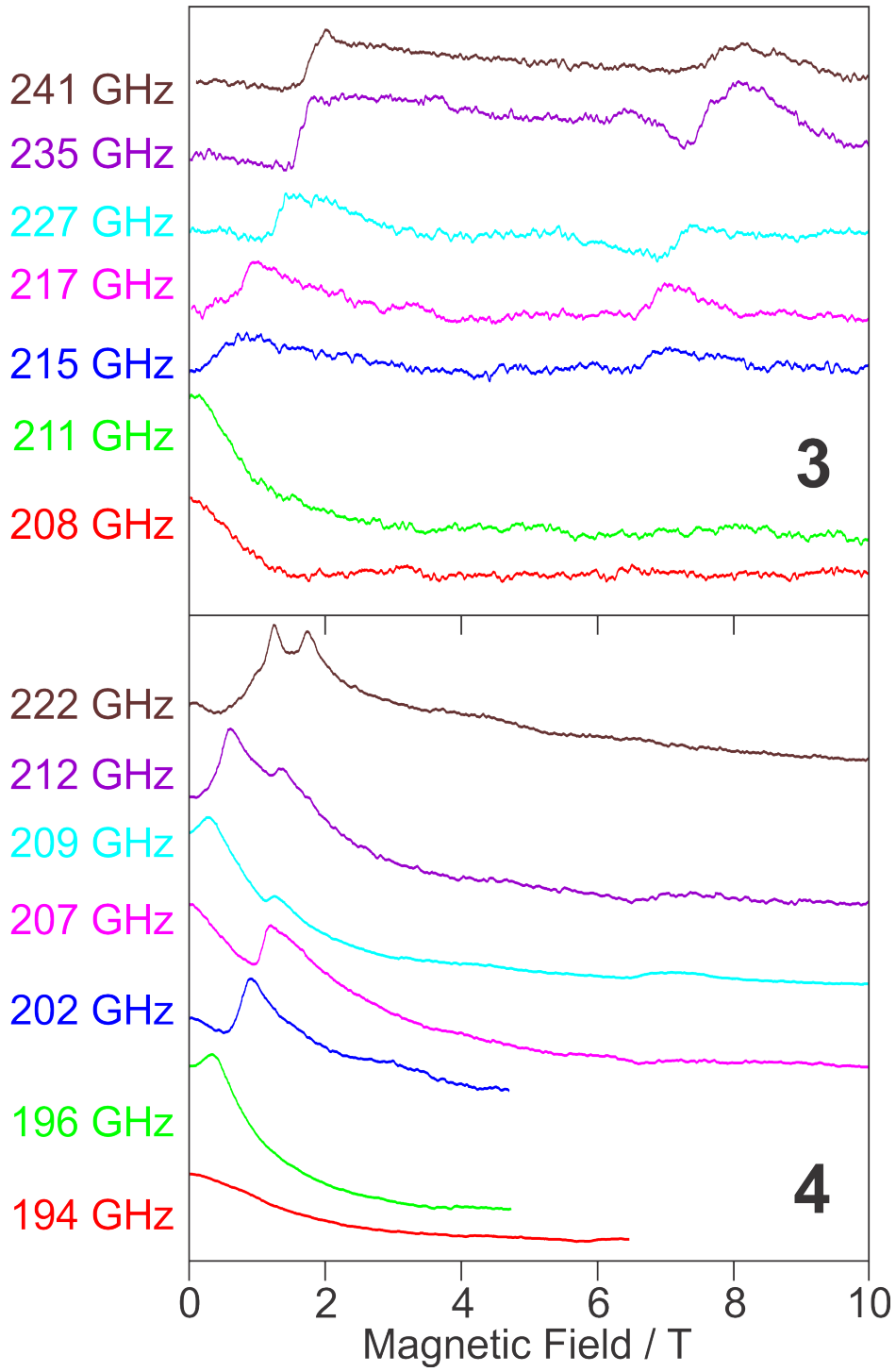

Figure 8. Selected HFEPR spectra of **3** (upper panel) and **4** (lower panel) obtained at 4.2 K using a resistive magnet and BWO sources at the frequencies indicated. The spectra were recorded near their respective zero-field transitions. Amplitudes are normalized within the series for a given complex. For **3**, the signal at 7 – 9 T is at g = 2 and may be due to a low-spin Fe(III) impurity.

Concerning compound **3**, both spectrometers delivered a single zero-field transition at ca. 210 GHz (Figure 8, upper panel), with no additional resonances detected under any other field and frequency conditions. However, at higher frequencies, the derivative spectrum (field modulated, superconducting magnet setup) again shows a splitting of this $\Delta M_S = \pm 2$ transition, this time into a doublet (or triplet, Figure S5, Supporting Information). In this case, the splitting clearly increases with frequency or field, and is thus attributed to *g* anisotropy, despite the axial nature of the **D** tensor. Full analysis of the 2D field-frequency data set for the two complexes (shown in Figure S6, Supporting Information) gave the spin Hamiltonian parameters summarized in Table 3. These parameters will be discussed in detail in the computational section below, but we note now that the $|D|$ values for the two complexes are similar,[134] ca. 7 cm^{-1}, which is much smaller in magnitude than that seen for oxidoiron(IV) complexes with $S = 1$ ground states ($D > +20$ cm^{-1}).[73, 133] However, these spin triplet $[FeO]^{2+}$ species have tetragonal symmetry; those with trigonal symmetry have spin quintet ground states, with $|D| \sim 5$ cm^{-1}.[135]

FT-FD THz EPR

The HFEPR spectra described above were recorded in the field domain, as is the case for EPR in general. The useful information, however, was contained largely in the field region near zero, but with varying microwave frequencies (Figure 8). What is therefore more desirable than approximating a zero-field frequency-domain experiment in this manner, is actually to perform such an experiment. This was indeed done for **3** and the resulting frequency domain spectra at zero-field and at various external fields are shown in Figure 9. At zero applied field, there is a single electronic resonance, located at 7.22(1) cm^{-1}, which directly corresponds to $|D|$ for a spin triplet. This value of $|D|$ obtained from frequency-domain measurements on **3** agrees to within 2% of the value obtained from field-domain (HFEPR) measurements. The ideal, single Gaussian

lineshape of this band (even at the highest resolution, 0.025 cm^{-1}) suggests that there is no doubling due to the presence of rhombic zfs, within its linewidth (0.1 cm^{-1}, hwhm). Thus, the system is essentially axial, also in agreement with HFEPR, as might be expected from its nearly trigonal symmetry.[136] This band greatly shifts and broadens with application of an external magnetic field, as expected for an electronic spin transition, as opposed to a vibrational mode that would unaffected by a magnetic field, so that it is no longer observable at $B_0 > 2$ T. Unfortunately, the quantitative analysis of this behavior is complicated by the apparent absence of parallel transitions (i.e., magnetic field along the **D** tensor *z* direction). Use of isotropic *g* values in the range 2.0 – 2.1 adequately model the observed behavior of what are assumed to be only perpendicular (i.e., magnetic field along the **D** tensor *xy* direction) transitions. A full understanding of the field dependence of these frequency domain signals is beyond the scope of this work, as among other aspects, it would require test compounds with precisely known *g* values and investigation of possible field orientation effects, requiring much more readily available (i.e., commercial) test compounds.

To relate the magnetic susceptibility and magnetic resonance experiments, we note that the susceptibility fits using a positive *D* value give its magnitude in rough agreement with the low temperature magnetic resonance techniques, while fits using a negative *D* value gave a large magnitude that is more in line with the zfs expected for a ^{3}E ground state. This behavior may be related to the pseudo-Jahn-Teller effect operative in **3**, and will be described in more detail below.

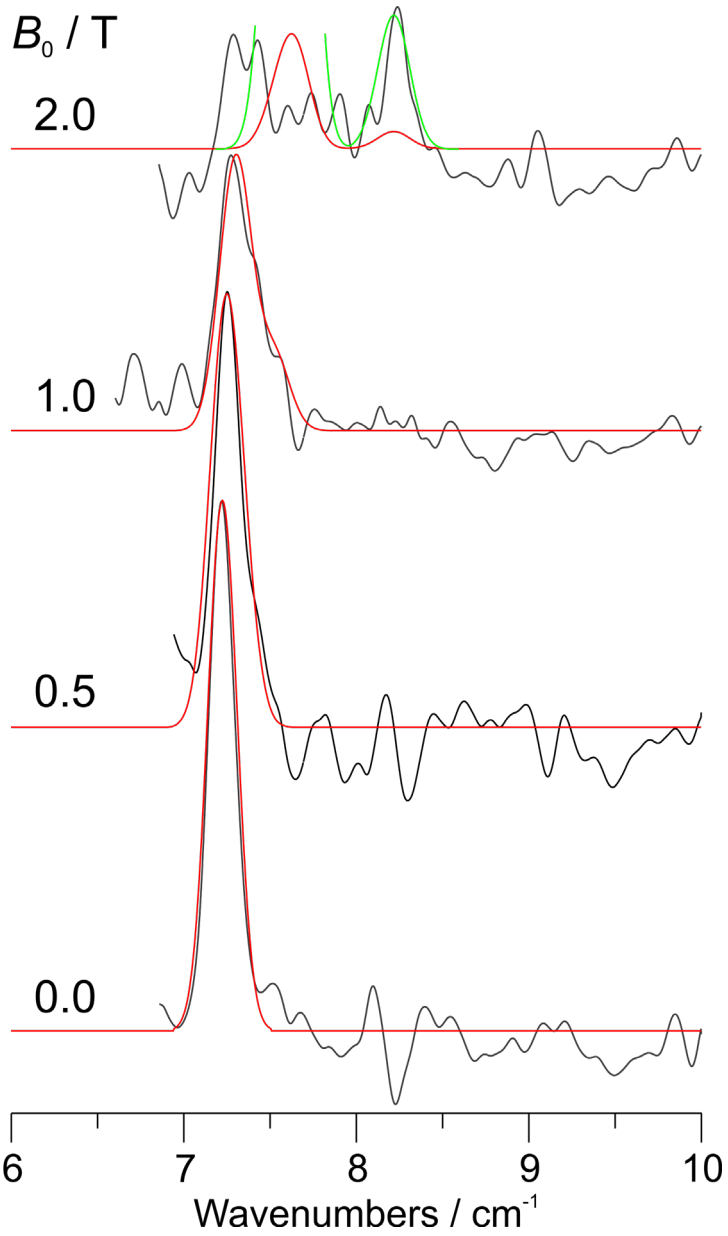

Figure 9. Experimental (black traces) and simulated (red and green traces) FT-FD THz-EPR spectra of **3** recorded at 5 K and varying applied magnetic fields as indicated. The experimental spectra were recorded under identical conditions, except for applied field, so their intensities correspond. The simulations use a spin Hamiltonian with $S = 1$, $|D| = 7.225$ cm^{-1}, $g_{iso} = 2.00$ and a Gaussian linewidth (hwhm) of 0.10 cm^{-1} (3.0 GHz). The instrumental resolution is 0.025 cm^{-1}. The simulation intensities are each scaled to match the corresponding experimental spectrum. The green simulated trace for $B_0 = 2$ T has been scaled to match the intensity of the higher energy feature; thus the lower energy feature is off-scale and truncated. The simulations do not use a full powder pattern (i.e., the full polar angle θ range), but only θ = 80 – 90° with ϕ = 0 – 90° (full range). Additional simulations are shown in Figure S7 (Supporting Information).

Table 3. Experimental (**3** and **4**) and calculated zfs and **g**-tensor data for $S = 1$ Fe(IV) imido complexes. (Theoretical coupled perturbed values are in parentheses.)

Comp-ound	Data type	Geometry	D / cm^{-1}	E / cm^{-1}	g_x	g_y	g_z
3	Exp (HFEPR)		|7.08(1)|	|0.05(10)|	2.07(1)	2.39(1)	--- [a]
	Exp (FD-THz EPR)		|7.22(1)|	|0.00(10)|	2.0 – 2.2 [b]	2.0 – 2.2 [b]	--- [a]
	Exp (DC susceptibility)		+14.5(5), –33.7(5) [c]	---	2.105 [c]	--- [c]	--- [c]
	BLYP	exp	–8.825 (–6.050)	–2.107 (–1.143)	2.016	2.023	2.101
	B3LYP	exp			2.019	2.032	2.151
	BLYP	opt	–7.537 (–4.747)	–1.981 (–1.080)	2.015	2.023	2.086
	B3LYP	opt			2.020	2.035	2.131
	CASSCF	opt	–45.187	–1.641	1.986	2.000	2.462
	sa-CASSCF	opt	–92.061	–1.986	1.932	1.947	2.855
4	Exp (HFEPR)		|6.71(1)|	|0.22(1)|	2.21(1)	2.19(1)	2.32(1)
	BLYP	opt	–7.562 (–4.763)	–2.117 (–0.143)	2.014	2.023	2.085
	B3LYP	opt			2.019	2.034	2.130
	CASSCF	opt	–45.107	–1.676	1.984	1.999	2.460
	sa-CASSCF	opt	–90.070	–2.006	1.934	1.949	2.839

[a] No value for g_z was obtained from either paramagnetic resonance technique.
[b] The FT-FD THz-EPR experiment did not allow definitive determination of g values, but suggests that g_x and g_y are in the range $2.0 \leq g_{x,y} \leq 2.2$.
[c] Fits to the magnetic susceptibility data yielded significantly different magnitudes of D depending on whether the fit was constrained to a positive or a negative value (see text). The fits used axial symmetry ($E \equiv 0$) and an isotropic g value fixed at 2.105 to match the higher temperature data; allowing g to vary led to it changing only minimally with little or no improvement in fit.

Ligand-field theory (LFT)

Classical ligand-field theory (LFT), using the angular overlap model (AOM),[137, 138] was previously applied to a spin quintet, trigonal, oxidoiron(IV) complex,[135] taking advantage of an earlier study that employed electronic absorption and MCD spectroscopies.[139] Here we can analogously make use of the previously reported analysis of the electronic absorption spectra for **1**.[33] The relevant aspects of this study, as well as how the AOM is applied in this case, are described in detail in Supporting Information. In brief, it is possible using a simple LFT model to arrive at the singlet spin ground state for **1** (and, due to their similarity, for **2** as well) with bonding parameters that are reasonable both for the nitrido N, making use of earlier studies on Cr and Mn nitrido complexes,[140, 141] and carbene C donor ligands.[142, 143] Moreover, the earlier analysis of the electronic transitions[33] is validated as well. It should be noted, however, that, especially with inclusion of spin-orbit coupling (SOC), the $^1A_1$ ground state of **1** is not described as a singlet in the simple, valence-bond sense of having two filled orbitals $\left(e_{(a)}{}^4 a_1{}^0 e_{(b)}{}^0\right)$; rather, there is significant populations of the higher orbitals, but with overall paired spins ($M_S = 0$). This finding is corroborated and expanded on in the QCT section that follows.

In the case of the imido complexes, **3** and **4**, the challenge is to obtain a spin triplet ground state, despite the superficial similarity between the imido and nitrido complexes in terms both of their structures and their electronic absorption spectra. We note that another trigonal four-coordinate Fe(IV) imido complex ($[\{PhB(P^{t}Bu)_2(pz')\}Fe^{IV}(NAd)]^+$;) exhibits an $S = 1$ ground state, so that the discussion here is generally applicable to these as well. There is a diamagnetic four-coordinate Fe(IV) imido complex,[36] but its geometry is quite different, namely *cis*-divacant octahedral so that its ideal symmetry is only C_s, thus with no orbital degeneracies.[144] As shown in the Supporting Information, however, the slight increase in θ angle (i.e., the angle between the

B-Fe-N, approximate C_3 axis, and the ligand carbene C atoms; see Scheme S1) between the imido complex **3** and the previously analyzed[33] nitrido complex **1**[145] is sufficient to lead to a ^{3}E ground state $\left(e_{(a)}{}^3 a_1{}^1 e_{(b)}{}^0\right)$ see Scheme 1 (left), ground state for **3**, without any other changes in bonding or Racah parameters (it is likely that the σ- and π-donation from the imido ligand is slightly weaker than that from the nitrido, see below). An orbitally non-degenerate, ^{3}A$_2$ ground state (Scheme 1, right), is not favored. LFT predicts triplet excited states, accessible via electric-dipole allowed transitions, with energies close to those of the singlet excited states calculated for the nitrido complex, thus the electronic absorption spectra are similar whether the ground state is a singlet or a triplet. The orbitally degenerate ^{3}E ground state is subject to a Jahn-Teller distortion, which may give rise to the zfs observed by HFEPR, but in a manner that is not well treated by the present, simple LFT model. QCT, as described below, can better handle these subtle effects.

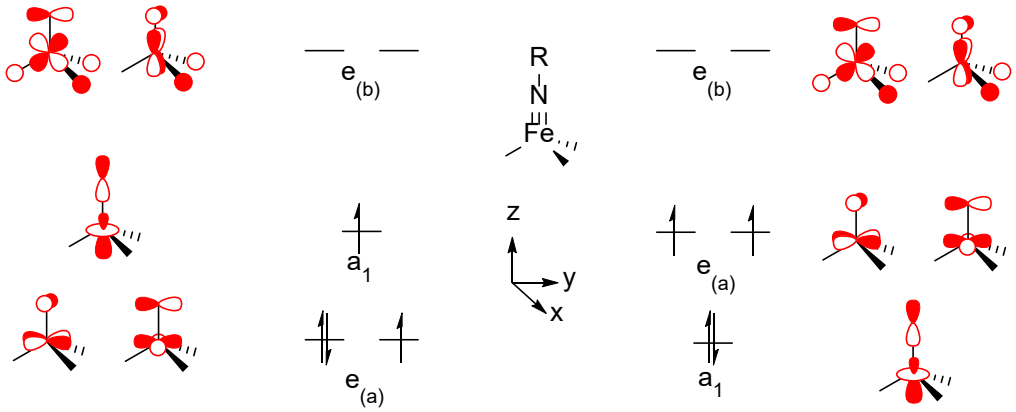

Scheme 1. Possible formal d-orbital occupation scenarios in trigonal ligand field for Fe(IV) imido complexes.

Quantum Chemical Theory (QCT)

In this section we first address the energetically-favored geometries and spin states, followed by a discussion of the EPR-derived parameters (i.e., zfs) and Mössbauer parameters and

conclude with a brief comparison of the electronic structure of the nitrido and imido complexes, particularly with respect to their ground state spin preferences, at the end of this QCT section.

Optimized geometries. We have performed B3LYP/6-311G* geometry optimization of the neutral molecules **1** and **2** as well as the singly charged cations of **3** and **4**[146] in the singlet, triplet, and quintet spin states. In agreement with experimental observations, **1** and **2** prefer the singlet spin state whereas **3** and **4** prefer the triplet spin state (Table S12). Since the relative energies of the other spin states indicate only vanishing populations, only the energetically preferred spin states will be discussed. The differences between experimental structural data and the optimized structures are compiled in Tables S13 and S14. Consistent with experimental data, the optimized iron imido structures do not retain the maximal possible C_s symmetry (a trigonal rotation axis is missing because of the phenyl group bonded to B atom) due to the pseudo-Jahn-Teller (PJT) effect. The consequences of this effect were observed by EPR earlier for the S = 1/2 iron(V) complex [{PhB(Im^{tBu})$_3$}FeN](BAr$_{F24}$), where [PhB(Im^{tBu})$_3$]$^-$ = phenyltris(3-*tert*-butylimidazol-2-ylidene),[147] which has a slightly bent B-Fe-N angle. The PJT effect in the cations of **3** and **4** is practically the same as in [PhB(^{t}BuIm)$_3$FeN]$^+$, but the doublet spin states must be replaced by triplets. Further comparison of the PJT effect in these Fe(V) and Fe(IV) complexes is given in Supporting Information.

Generally speaking, all bond lengths and/or interatomic distances between iron and the ligating atoms (including formally also boron) are shorter for the nitrido than the imido compounds. This suggests that the one σ and two π dative bonding picture of the [Fe-N]$^+$ moiety of nitrido compounds (**1** and **2**) yields a stronger bond compared to the [Fe-NR′] imido compounds (**3** and **4**). Interestingly, the stronger Fe-N dative interactions in **1** and **2** increases the

electron density at the central Fe atom (see below) which is manifested in the shorter interatomic distances.[148]

Quantum Theory of Atoms in Molecules (QTAIM) analysis. For the sake of simplicity we will generally restrict discussion of our QTAIM B3LYP/6-311G* study to the most preferred spin states of these complexes (Tables S15 – S18). As mentioned above, the QTAIM charge on Fe is larger in the cations **3** and **4** than in **1** and **2**. An interesting observation is that, unlike the imido complexes, for which the cations of **3** and **4** have nearly equal N_{imido} atomic volumes and charges, these properties of the nitrido ligands are sensitive to tris(carbene)borate ligand substituent (R). Specifically, the $N_{nitrido}$ in **1** (R = ^{t}Bu) has a smaller atomic volume and a more negative charge than in **2** (R = Mes), which suggests that the nitrido ligand in **1** should be more reactive, counter to experimental observations. However, while the ^{t}Bu groups in **1** effectively shrink the volume of the nitrido ligand, increasing its charge density, they also screen interactions with substrates and reduce its reactivity as compared with **2** where there is essentially no steric hindrance between $N_{nitrido}$ and R = Mes.

Bond critical point (BCP) analysis (as well as the electron density integrated over the mutual interatomic surfaces) reveals that the Fe - $N_{nitrido}$ bonds in **1** and **2** are stronger than the corresponding Fe - N_{imido} bonds in cations **3** and **4**, see Tables S16 and S17. The vanishing BCP ellipticity agrees with a bonding interaction composed of one σ and two almost equivalent perpendicular π interactions (see below). More positive BCP Laplacian values of all Fe - N_{imido} than for the Fe – $N_{nitrido}$ bonds indicate a greater degree of electron density transfer between iron and the imido ligand. While this seems counter-intuitive based on the assumption that the Fe – $N_{nitrido}$ dative bond is stronger, this is caused by the contributions of the perpendicular negative eigenvalues of the Hessian which are twice as negative for the Fe – $N_{nitrido}$ (ca. -0.70 e/bohr^5)

than the Fe - N_{imido} (ca. –0.33 e/bohr^5) bonds, see Table S18, i.e., the perpendicular π donor-acceptor interactions are more pronounced for the nitrido complexes. The dominating positive eigenvalue in the bond direction is slightly larger for Fe – $N_{nitrido}$ (ca. 1.80 e/bohr^5) than Fe - N_{imido} (ca. 1.67 e/bohr^5), which favors a shorter and stronger bond with a slightly more convex distribution of the electron density along this bond.

We have not found any Fe - B bond path (see Figure S15, Supporting Information). The absence of this bonding interaction is supported from the QTAIM prospective by the presence of a cage critical point (i.e. a local electron density minimum) in the center of the B(μ-imidazolylidene)$_3$Fe cage for all complexes. Further details on QTAIM results are provided in Supporting Information.

Spin Hamiltonian parameters. The theoretical spin Hamiltonian parameters (zfs and *g* values) are compiled in Table 3. The agreement between theoretical and experimental values is indeed reasonably good in the case of BLYP/TZVP results (considering the absolute value), where the QRO method yields better agreement with experiment comparing to CP level of theory. Nevertheless, the CASSCF(10,8)/TZVP results of **4** (note that these are almost identical to those of **3**, see Table 3), based on state averaging of the 50 quintet, 100 triplet, and 100 singlet states included in the final zfs evaluation, yields a *D* value that is six times larger in the absolute value than found in the EPR experiments. Here, quintet, triplet, and singlet states contributions for **4** are –0.332, –45.737 and +1.215 cm^{-1}, respectively. Among these, the contribution of the first triplet excited state is –49.682 cm^{-1}, which is best described as a $3d_{xy}^{\ 1}d_{x^2-y^2}^{\ 2}d_{z^2}^{\ 1}$ determinant (weight, defined as $c_1^* c_1 = 0.712$). The dominant configuration space determinant in the ground state CASSCF(10,8)/TZVP wave function has a $3d_{xy}^{\ 2}d_{x^2-y^2}^{\ 1}d_{z^2}^{\ 1}$ character ($c_0^* c_0 = 0.736$) and the energy difference between the ground and first excited state is 2448 cm^{-1}. When performing

CASSCF state averaging for the two lowest triplet states, the overall *D* value is twice as large as in the case of state specific calculations. The CASSCF results are described at the end of this section. A large zfs value (i.e., a splitting between the two lowest energy levels), 69.9 cm^{-1}, is found in the LFT analysis as well (see Supporting Information, including Table S11). The discrepancy between CASSCF and LFT theory when comparing to the experimentally fitted parameters of the Spin Hamiltonian of the EPR experiments is rather discouraging and offers an additional impetus to improvements in theory. A recent example of a similar kind of difficulty was reported in the calculation of zfs parameters of Fe(III) porphyrin complexes with axial halido ligands (high-spin $3d^5$ configuration).[149] The obvious remedy here would be the inclusion of dynamic correlation by either a complete active space second order perturbation theory (CASPT2)[150-152] or an N-electron valence state perturbation theory (NEVPT2)[153-155] treatment. These methods have been recently applied to a variety of transition metal ion complexes with $S > 1/2$, such as of M(I) (M = Cr, Mn, Co)[156] and Co(II).[157-159] Unfortunately, such a treatment here was not possible on the bona fide systems and treatment of a truncated system did not yield a *D* value any closer to experiment. It has to be pointed out, albeit on the premise of "getting the right answer for the wrong reason", that the CASSCF(10,7) calculation that involves breaking the equal description (close degeneracy) of the $e_{(b)}$ MOs yields a *D* value of –9.23 cm^{-1} for **4**, which is close to the experimentally derived value (leaving the sign of the *D* parameter out of consideration, which was not well determined experimentally). In addition, a CASSCF(8,7) calculation which excluded $3d_{xy}$(Fe) from the CASSCF space yielded a positive contribution to $D = +3.14$ cm^{-1}, of 50 triplet states but a negative contribution to $D = –5.38$ cm^{-1} of 50 singlet states to give the net *D* value of –2.624 cm^{-1}. Despite the improved agreement between the CASSCF(10,7) or CASSCF(8,7) results and the experimental *D* value, this rather artificially

enforced $e_{(b)}$ or $e_{(a)}$ symmetry breaking will not be considered any further, but for one remark. It appears that the smaller *D* value (in absolute value) derived from low temperature magnetic (both susceptibility and resonance) measurements can be attributed to a distorted geometry that breaks the ^{3}E symmetry (most probably due to JT effects; not to be confused with the orbital order of Scheme 1, right). However, ^{3}E-like symmetry seems to be effectively restored at higher temperature (e.g., a kind of vibrational effect) as found in the preference for a negative *D* value of the susceptibility data fit above 10 K – a temperature regime that was not amenable to paramagnetic resonance measurements.

An additional option to explain the shift of the CASSCF(10,8) results is the possibility of bending and hence further enforcement of JT distortion (which is true for simplified complexes with replacing Mes groups by hydrogens or methyl groups and using methyl groups instead ^{t}Bu or Ad). A bent nitrido geometry has been already obtained by Tangen et al.[52] When enforcing bending of the C-Fe-$N_{nitrido}$ angle to about 150° in **4**, the CASSCF(10,8)/VTZP-calculated *D* value becomes equal to −17.54 cm^{-1}. The above mentioned linearity arises due to the contributions of two different parts of the adiabatic potential obtained by splitting the (pseudo)degenerate electron states. The ground state of the complex is described by the lower part of this potential in the shape of a warped "Mexican hat" with local minima corresponding to stable structures fully breaking the degeneracy at low temperatures. Bulky Mes groups might affect this potential slope and reduce the barriers between individual stable potential minima corresponding to bent structures and thus support the dynamical averaging of the less symmetric bent configurations into the high symmetric linear structure observed at higher temperatures which is known as a dynamical (P)JT effect (see also the discussion in Supporting Information). This behavior is consistent with the results of an imido model compound with hydrogen or

methyl groups in the position of the supporting bulky Mes groups and is fully supported by the results of Tangen et al.[52] (see discussion in Supporting Information). The energetically upper adiabatic potential part, with a formally normal umbrella shape, resides over the Mexican hat and its slope is affected by the presence of the bulky Mes groups as well. No dynamical effects are necessary to explain the corresponding symmetric structure, but it corresponds to a higher electronic state and its probability (and thus the its contribution to the structure observed) is much lower than of the above mentioned ground state.

The BLYP/TZVP and B3LYP/TZVP calculations yield **g** matrix diagonal components shifted from the experimental ones, but it must be noted that the latter are not well determined, in particular their direction in the molecular framework (see Table 3). The HFEPR studies do suggest that one **g** matrix component is relatively large in magnitude; combining with the susceptibility indicating an average *g* value of 2.10, so **g** ≈ [2.0, 2.0, 2.3] is reasonable for a consensus with the experimental **g** matrix. The g_x and g_y values are close to 2.0 and only the *z* component is shifted to 2.09 and 2.13 in the case of BLYP and B3LYP functionals, respectively, using the optimized geometry. The CASSCF(10,8) calculation yields a *g* value close to 2.0 in the case of the g_x and g_y components, but the g_z component is found close to 2.5 (this value is 2.9 in the case of the state-averaged CASSCF calculation).[160]

Mössbauer. Theoretical B3LYP/TZVP/COSMO(water) Mössbauer parameters are enumerated along with their accompanying experimental values in Table 2. Both the theoretical and experimental Mössbauer isomer shifts (δ) are more negative for the nitrido complexes (**1** and **2**) than the imido complexes (**3** and **4**). Similarly, larger quadrupole splittings (ΔE_Q) are observed for the nitrido than for imido complexes. The calculated values of the species under study show reasonable agreement with the experimental results, as has been previously observed,[112] which

validates the theoretical model. The inclusion/exclusion of the extra solvent molecule in the proximity of N_{imido} atom within the experimental structure of **1·MeCN** has no impact on the theoretically determined Mössbauer parameters, despite the fact that modest differences in these parameters between **1** and **1·MeCN** are experimentally observed. We therefore attribute these differences to ligand field changes that are due to solid state packing effects rather than direct interactions between the nitrido complex and MeCN. The difference in Mössbauer isomer shift between imido and nitrido compound classes can be assigned to differences in the spin states and bonding interactions, rather than to differences in the physical oxidation state. B3LYP/TZVP/COSMO(water) contact densities at the nucleus (ρ_{NUC}) which were used to calculate the Mössbauer isomer shifts according to Römelt et al.[112] are shown in Table S19 (Supporting Information).

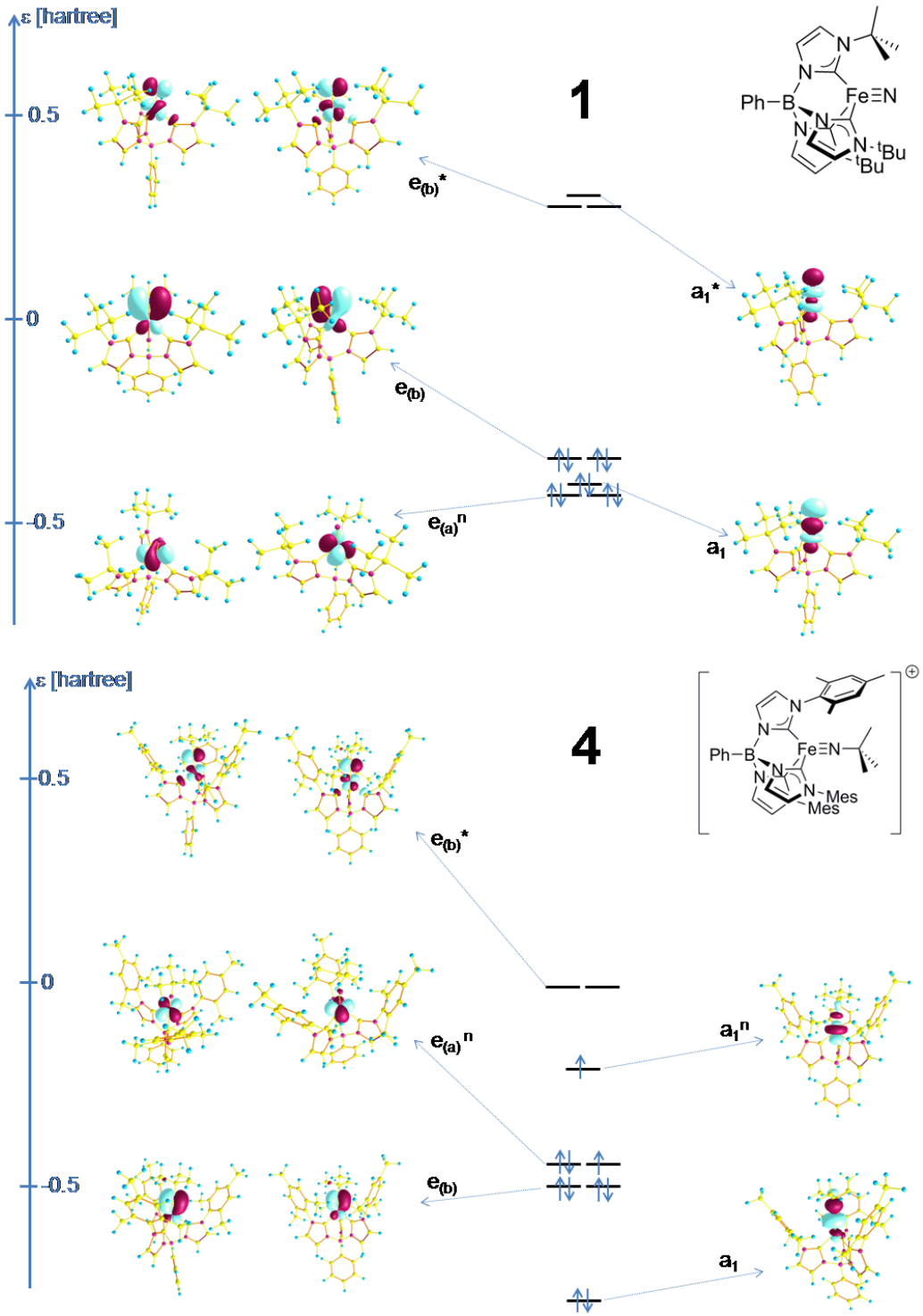

Scheme 2. NBO diagrams of **1** (top, CASSCF) and **4** (bottom, sa-CASSCF). NBOs of **1** and **4** are positioned accordingly to their eigenvalues (ε) following the ε axis labeling. The up/down occupation arrows reflect the configuration of the dominant determinant from the CASSCF space. Cyan, pink, yellow, violet and silver spheres represent H, B, C, N and Fe atoms, respectively.

Spin state preferences. The qualitative agreement (as well as differences) between the DFT and CASSCF results from the orbital and Mulliken population perspectives is provided in the Supporting Information. Efforts to elucidate the differences in spin state preferences in the nitrido (**1**, **2**) and imido (**3**, **4**) species will be described below. We will first consider the orbitals (eigenvalues/energies) of the individual imido and nitrido ligands. In the nitrido case, one has to formally assume an N^{3-} ligand/group with the 2s/2p orbitals having higher and more positive Hartree-Fock/TZVP [161] eigenvalues (0.11 / 0.65 hartree) than the $^{t}BuN^{2-}$ imido ligand of **4** (-0.21, -0.24, 0.06, and 0.07 hartree in the case of MOs with 2s, $2p_z$, $2p_x$, and $2p_y$ AO character of nitrogen, respectively), see Scheme S1. It is noteworthy that the σ-bonding 2s(N) and $2p_z$(N) orbitals of the $R'N^{2-}$ ligand are close in energy and the two perpendicular $2p_{x,y}$(N) orbitals interact with orbitals on the tertiary carbon atom (not shown). The eigenvalues of the $^{t}BuN^{2-}$ ligand are considerably lower in energy due to the less negative charge of this ligand as well as stabilization of the nitrogen AOs via bonding with the ^{t}Bu group. Thus, stabilization of the $2p_z$(N) AO density in the R′-N bond reduces its ability to participate in σ(Fe-N) interactions, as compared with the corresponding $2p_z$(N) AO of the N^{3-} ligand, which also has a more negative overall charge.

To discuss spin state preferences in the imido and nitrido complexes, we consider the Fe d^4 electronic configuration in formal C_{3v} symmetry, where the nitrido and imido ligands are apical to the (nearly) trigonal pyramid base composed of the iron(IV) ion and the tris(carbene)borate ligand. Following Schemes 1, 2, and S1, the ligand field electronic configuration of iron in the complexes has (formally) doubly degenerate $e_{(a)}$ orbitals, with an a_1 orbital singly occupied in the triplet state, whereas the $e_{(b)}$ (formally) doubly degenerate orbitals are involved in the bonding and antibonding π-interactions with the nitrido/imido ligand. The

four d-electrons of Fe will occupy different spin-orbitals and have the largest possible multiplicity when the $e_{(a)}$ to a_1 energy gap is small enough (imido case); these electrons pair up within the $e_{(a)}$ NBOs[162] when the energy gap is sufficiently large (nitrido case). Thus one could consider the nitrido and imido ligands from a spectrochemical series perspective with the imido splitting the $e_{(a)}$ and a_1 orbitals to a lesser extent than for the nitrido ligand.

Nevertheless, the QCT picture, which is based on the NBOs of **1** and **4**, has to take into account the relative energies and order of the a_1 d_{z2}(Fe)-like NBO with respect to $e_{(a)}$ d(Fe) orbitals, as well as the overall character of NBOs (Scheme 2 and S1). For complex **4**, the Fe(d_{z^2})$^{\cdots}$N-R′$^{2-}$ bonding NBO (a_1) has the lowest eigenvalue (see Scheme 2 and S1, Figure S16b or Table S21), but is predominantly imido $2p_z$ in character. By contrast, the second highest a_1 NBO in the [Fe(d_{z^2})$^{\cdots}$N-R′$^{2-}$] moiety is non-bonding $3d_{z^2}$ (Fe) in nature, well-suited to host an unpaired electron as it is energetically close to the $e_{(a)}$ NBOs. In the case of **1**, the a_1 Fe(d_{z^2})$^{\cdots}$N^{3-} bonding interaction does not have such a small eigenvalue, but amounts to almost one $3d_{z^2}$ electron (see Schemes 2 and S1, Figure S13e). In the case of the nitrido ligand, the negative charge from the $2p_z$(N^{3-}) AO, with its high eigenvalue, is donated into the bonding a_1 orbital of **1**, due to large and favorable energy and spatial/charge gradients, but the bonding nature of this NBO makes it unsuited to host an open shell. The a_1* NBO of **1** is purely antibonding and has a high eigenvalue, see Scheme 2 and S1. Thus, this a_1* NBO is also far from being suited to host the open shell electron, being far from the $e_{(a)}$ NBOs of the d^4(Fe) configuration. Despite the different spin states and the nature of the lowest a_1 NBO, the four non-bonding 3d electrons identify the formal oxidation state of the central atom to be Fe(IV) in both the nitrido and imido complexes. The oxidation state assignment for the imido complex is in contrast with the assignment made by Iovan and Betley in their dipyrrinato complex, namely

Fe(III)-iminyl radical.[38] We speculate that this difference might be related to fact that in **3** and **4** (and in the previously reported diphosphine-pyrazolyl complex[27]) the imido substituent is aliphatic (R′ = Ad, ^{t}Bu), while in the dipyrrinate, it is aromatic (R′ = C_6H_3-2,6-$^{i}Pr_2$) and easier to reduce. Further synthetic efforts are needed to test this hypothesis.

The order of orbitals in the nitrido (**1**) and imido (**4**) compounds is also worth highlighting. The $e_{(b)}$ Fe(d_{xz} / d_{yz})···N-R′$^{2-}$ bonding orbitals in **4**, when enforcing CASSCF(10,8) state averaging between Fe(d_{xy}) and Fe($d_{x^2-y^2}$) NBOs, are shifted energetically below the non-bonding Fe(d_{xy}) and Fe($d_{x^2-y^2}$) NBOs. Hence, $e_{(a)}$ Fe(d_{xy}) and Fe($d_{x^2-y^2}$) NBOs are neighboring with the non-bonding a_1 Fe(d_{z2}) in the active space. On the other hand, in the case of **1**, the bonding interactions in the $e_{(b)}$ and a_1 NBOs are energetically above the non-bonding Fe(d_{xy}) and Fe($d_{x^2-y^2}$) NBOs and the antibonding a_1* is the highest NBO in the active space.

Conclusion

This paper has reported the results of a comprehensive experimental and computational investigation into the electronic structure of iron(IV) nitrido {FeN}$^{+}$ and imido {FeNR′}$^{2+}$ complexes in three-fold symmetry. The experimental techniques included magnetometry, ^{57}Fe Mössbauer spectroscopy – ideally suited for these complexes, and both field- and frequency domain low temperature paramagnetic resonance (HFEPR and FD-FT THz-EPR, respectively) spectroscopy, ideally suited for the integer spin (S = 1) imido complexes, with their significant zfs. Results of these spectroscopic studies have provided a platform for experimentally correlated electronic structure calculations that address the spin state preferences of the two sets of complexes. Specifically, the Mössbauer results show the utility of the isomer shift in the Fe(IV)

assignment for these imido and nitrido complexes, as opposed to other formal oxidation states, which was further validated by QCT. Concerning the magnetometry and magnetic resonance spectroscopic studies, which probed the zfs of the spin triplet imido complexes, the results were more ambiguous. The small magnitude, positive *D* value derived from low temperature magnetic susceptibility and EPR data contrast with the negative and large magnitude *D* value derived from higher temperature (above 10 K) susceptibility measurements. A way out of this conundrum is offered by the *ab initio* findings, which indicate ^{3}E symmetry breaking / restoring due to (P)JT effect in a relatively tight temperature window. Future experiments including low temperature crystallography and more extensive magnetometric and spectroscopic measurements may need to be performed to test this hypothesis.

The details of the spectroscopic investigations are of interest, but the main point is that despite their differences in charge, the spin state preferences of the two sets of complexes can be directly ascribed to the donor properties of the imido and nitrido ligands. Although both ligands can bind to iron through one σ- and two π-symmetry interactions, a critical difference between the two is the lower σ-donor ability of the imido ligand that is a consequence of stabilizing interactions with its substituent (R′ = alkyl group). This factor, along with the smaller charge of the imido ligand, reduces the energy of the σ-interactions with the iron center, most significantly lowering the energy of the out-of-phase a_1 $\left(d_{z^2}\right)$ orbital and decreasing the energy gap between the $e_{(a)}$ and a_1 orbitals. Thus, the imido complexes exhibit a ground state electronic configuration that can be described formally as $\left(d_{xy}, d_{x^2-y^2}\right)^3 d_{z^2}{}^1$, while the nitrido complexes are $\left(d_{xy}, d_{x^2-y^2}\right)^4 d_{z^2}{}^0$, with respect to the non-bonding 3*d* orbitals of the central iron atom.

Whether the present type of imido complex can be made into a spin singlet and the nitrido into a spin triplet is an open question. The R′ employed here is already strongly donating, so an increase in imido σ-donor strength is challenging. On the other hand, it may be possible to modify the donor strength of the nitrido ligand, e.g., by Lewis acid coordination.[163-165]

In any case, it the relative energy and character of the *single orbital* type (a_1) that dictates the resulting spin state of the complex. More generally, the σ-donor ability of the apical ligand is therefore a sufficient parameter for tuning the spin states of (formally) d^4 complexes in three-fold symmetry and apical ligands of appropriate σ-donor strength are expected to facilitate $S = 0/S = 1$ spin state transitions. Such fundamental understanding of the ability of coordination chemistry to control spin state has relevance to the design of spin-based molecular devices.

ASSOCIATED CONTENT

Supporting Information. Synthesis; X-ray crystallographic data for **1** and **2**; Detailed description of Mössbauer dynamics; Additional Mössbauer spectra; Additional HFEPR spectra and analysis; Additional FT-FD-THz-EPR analysis; Discussion of LFT (AOM) for [{PhB(Im^R)$_3$}FeN(R′)]; Discussion of Pseudo-Jahn-Teller (PJT) effect in Fe(IV, V) nitrido, imido complexes; Background on QTAIM; Discussion of Molecular orbital (MO) pictures; Structure of model complex [{PhB(Im)$_3$}Fe(NCH_3)]; Molecular Orbitals from QCT calculations and Further Details from QCT calculations. This material is available free of charge via the Internet at http://pubs.acs.org.

AUTHOR INFORMATION

Corresponding Authors

* Joshua Telser: jtelser@roosevelt.edu; Jeremy M. Smith: smith962@indiana.edu.

Author Contributions

All authors have given approval to the final version of the manuscript.

Notes

The authors declare no competing financial interest.

ACKNOWLEDGMENTS

Funding from Indiana University and the US Department of Energy – Basic Energy Sciences (DE-FG02-08ER15996) is gratefully acknowledged. The Bruker X-ray diffractometer was purchased via a National Science Foundation (NSF) CRIF:MU award to the University of New Mexico (CHE04-43580). Work in the Harris lab (J.A.D. and T.D.H.) was supported by the NSF through Grant DMR-1351959 and Northwestern University. The HFEPR studies were supported by the NHMFL, which is funded by the NSF (Cooperative Agreement DMR 1157490), the State of Florida, and DOE. FD-FT THz-EPR measurements were obtained within BESSY II user service. We thank Dr. Eckhard Bill (MPI CEC, Mülheim) for assistance with the field-dependent Mössbauer measurements. We thank Prof. Robert Bittl (FU Berlin) for permitting measurements at the FD-FT THz-EPR setup and the Deutsche Forschungsgemeinschaft (DFG) for funding within priority program SPP 1601. We also thank Dr. Azar Aliabadi (HZB) for additional, high-resolution FD-FT THz-EPR measurements. The computational studies were supported by the Slovak Grant Agency VEGA under contract no. 1/0598/16. We thank the HPC center at the Slovak University of Technology in Bratislava, which is a part of the Slovak Infrastructure of

High Performance Computing (SIVVP Project ITMS 26230120002, funded by the European Region Development Funds), for computing facilities. J.N. acknowledges funding by the DFG through a research fellowship (grant no. NE 2064/1-1 FOR).

REFERENCES

1. Berry, J. F., Terminal Nitrido and Imido Complexes of the Late Transition Metals. *Comments Inorg. Chem.* **2009**, *30*, 28-66.
2. Smith, J. M., Strongly donating scorpionate ligands. *Comments Inorg. Chem.* **2008**, *29*, 189-233.
3. Ertl, G., Heterogeneous catalysis on the atomic scale. *Chem. Rec.* **2001**, *1*, 33-45.
4. Hoffman, B. M.; Dean, D. R.; Seefeldt, L. C., Climbing Nitrogenase: Toward a Mechanism of Enzymatic Nitrogen Fixation. *Acc. Chem. Res.* **2009**, *42*, 609-619.
5. Smith, J. M.; Subedi, D., The structure and reactivity of iron nitride complexes. *Dalton Trans.* **2012**, *41*, 1423-1429.
6. Lucas, R. L.; Powell, D. R.; Borovik, A. S., Preparation of Iron Amido Complexes via Putative Fe(IV) Imido Intermediates. *J. Am. Chem. Soc.* **2005**, *127*, 11596-11597.
7. Verma, A. K.; Nazif, T. N.; Achim, C.; Lee, S. C., A Stable Terminal Imide on Iron. *J. Am. Chem. Soc.* **2000**, *122*, 11013-11014.
8. Mehn, M. P.; Peters, J. C., Mid- to high-valent imido and nitrido complexes of iron. *J. Inorg. Biochem.* **2006**, *100*, 634-643.
9. Hohenberger, J.; Ray, K.; Meyer, K., The biology and chemistry of high-valent iron-oxo and iron-nitrido complexes. *Nat Commun* **2012**, *3*, 720.
10. Saouma, C. T.; Peters, J. C., ME and ME complexes of iron and cobalt that emphasize three-fold symmetry (E = O, N, NR). *Coord. Chem. Rev.* **2011**, *255*, 920-937.
11. Bart, S. C.; Lobkovsky, E.; Bill, E.; Chirik, P. J., Synthesis and Hydrogenation of Bis(imino)pyridine Iron Imides. *J. Am. Chem. Soc.* **2006**, *128*, 5302-5303.
12. Cowley, R. E.; DeYonker, N. J.; Eckert, N. A.; Cundari, T. R.; DeBeer, S.; Bill, E.; Ottenwaelder, X.; Flaschenriem, C.; Holland, P. L., Three-Coordinate Terminal Imidoiron(III) Complexes: Structure, Spectroscopy, and Mechanism of Formation. *Inorg. Chem.* **2010**, *49*, 6172-6187.
13. King, E. R.; Hennessy, E. T.; Betley, T. A., Catalytic C−H Bond Amination from High-Spin Iron Imido Complexes. *J. Am. Chem. Soc.* **2011**, *133*, 4917-4923.
14. Bowman, A. C.; Milsmann, C.; Bill, E.; Turner, Z. R.; Lobkovsky, E.; DeBeer, S.; Wieghardt, K.; Chirik, P. J., Synthesis and Electronic Structure Determination of N-Alkyl-Substituted Bis(imino)pyridine Iron Imides Exhibiting Spin Crossover Behavior. *J. Am. Chem. Soc.* **2011**, *133*, 17353-17369.
15. Cowley, R. E.; Holland, P. L., Ligand Effects on Hydrogen Atom Transfer from Hydrocarbons to Three-Coordinate Iron Imides. *Inorg. Chem.* **2012**, *51*, 8352-8361.
16. Ni, C.; Fettinger, J. C.; Long, G. J.; Brynda, M.; Power, P. P., Reaction of a sterically encumbered iron(I) aryl/arene with organoazides: formation of an iron(V) bis(imide). *Chem. Commun.* **2008**, 6045-6047.
17. Zhang, H.; Ouyang, Z.; Liu, Y.; Zhang, Q.; Wang, L.; Deng, L., (Aminocarbene)(Divinyltetramethyldisiloxane)Iron(0) Compounds: A Class of Low-Coordinate Iron(0) Reagents. *Angew. Chem. Int. Ed.* **2014**, *53*, 8432-8436.
18. Wang, L.; Hu, L.; Zhang, H.; Chen, H.; Deng, L., Three-Coordinate Iron(IV) Bisimido Complexes with Aminocarbene Ligation: Synthesis, Structure, and Reactivity. *J. Am. Chem. Soc.* **2015**, *137*, 14196-14207.

19. Brown, S. D.; Peters, J. C., Ground-State Singlet L_3Fe-(μ-N)-FeL_3 and $L_3Fe(NR)$ Complexes Featuring Pseudotetrahedral Fe(II) Centers. *J. Am. Chem. Soc.* **2005**, *127*, 1913-1923.
20. Moret, M.-E.; Peters, J. C., Terminal Iron Dinitrogen and Iron Imide Complexes Supported by a Tris(phosphino)borane Ligand. *Angew. Chem. Int. Ed.* **2011**, *50*, 2063-2067.
21. Brown, S. D.; Betley, T. A.; Peters, J. C., A Low-Spin d^5 Iron Imide: Nitrene Capture by Low-Coordinate Iron(I) Provides the 4-Coordinate Fe(III) Complex $[PhB(CH_2PPh_2)_3]Fe{:}N$-*p*-tolyl. *J. Am. Chem. Soc.* **2003**, *125*, 322-323.
22. Mehn, M. P.; Brown, S. D.; Jenkins, D. M.; Peters, J. C.; Que, L., Jr., Vibrational Spectroscopy and Analysis of Pseudo-tetrahedral Complexes with Metal Imido Bonds. *Inorg. Chem.* **2006**, *45*, 7417-7427.
23. Lu, C. C.; Saouma, C. T.; Day, M. W.; Peters, J. C., Fe(I)-Mediated Reductive Cleavage and Coupling of CO_2: An Fe^{II}(μ-O,μ-CO)Fe^{II} Core. *J. Am. Chem. Soc.* **2007**, *129*, 4-5.
24. Kuppuswamy, S.; Powers, T. M.; Johnson, B. M.; Bezpalko, M. W.; Brozek, C. K.; Foxman, B. M.; Berben, L. A.; Thomas, C. M., Metal–Metal Interactions in C_3-Symmetric Diiron Imido Complexes Linked by Phosphinoamide Ligands. *Inorg. Chem.* **2013**, *52*, 4802-4811.
25. Kuppuswamy, S.; Powers, T. M.; Johnson, B. M.; Brozek, C. K.; Krogman, J. P.; Bezpalko, M. W.; Berben, L. A.; Keith, J. M.; Foxman, B. M.; Thomas, C. M., One-Electron Oxidation Chemistry and Subsequent Reactivity of Diiron Imido Complexes. *Inorg. Chem.* **2014**, *53*, 5429-5437.
26. Nieto, I.; Ding, F.; Bontchev, R. P.; Wang, H.; Smith, J. M., Thermodynamics of Hydrogen Atom Transfer to a High-Valent Iron Imido Complex. *J. Am. Chem. Soc.* **2008**, *130*, 2716-2717.
27. Thomas, C. M.; Mankad, N. P.; Peters, J. C., Characterization of the Terminal Iron(IV) Imides $\{[PhBP^{tBu2}(pz')]Fe^{IV}{:}NAd\}^+$. *J. Am. Chem. Soc.* **2006**, *128*, 4956-4957.
28. Smith, J. M., Reactive Transition Metal Nitride Complexes. In *Prog. Inorg. Chem.*, Karlin, K. D., Ed. John Wiley & Sons, Inc.: 2014; Vol. 58, pp 417-470.
29. Betley, T. A.; Peters, J. C., A Tetrahedrally Coordinated $L_3Fe{-}N_x$ Platform that Accommodates Terminal Nitride ($Fe^{IV}{:}N$) and Dinitrogen ($Fe^{I}{-}N_2{-}Fe^{I}$) Ligands. *J. Am. Chem. Soc.* **2004**, *126*, 6252-6254.
30. Hendrich, M. P.; Gunderson, W.; Behan, R. K.; Green, M. T.; Mehn, M. P.; Betley, T. A.; Lu, C. C.; Peters, J. C., On the feasibility of N_2 fixation via a single-site Fe^{I}/Fe^{IV} cycle: Spectroscopic studies of $Fe^{I}(N_2)Fe^{I}$, $Fe^{IV}{\equiv}N$, and related species. *Proc. Natl. Acad. Sci. USA* **2006**, *103*, 17107-17112.
31. Rohde, J.-U.; Betley, T. A.; Jackson, T. A.; Saouma, C. T.; Peters, J. C.; Que, L., Jr., XAS Characterization of a Nitridoiron(IV) Complex with a Very Short Fe−N Bond. *Inorg. Chem.* **2007**, *46*, 5720-5726.
32. Vogel, C.; Heinemann, F. W.; Sutter, J.; Anthon, C.; Meyer, K., An Iron Nitride Complex. *Angew. Chem. Int. Ed.* **2008**, *47*, 2681-2684.
33. Scepaniak, J. J.; Fulton, M. D.; Bontchev, R. P.; Duesler, E. N.; Kirk, M. L.; Smith, J. M., Structural and Spectroscopic Characterization of an Electrophilic Iron Nitrido Complex. *J. Am. Chem. Soc.* **2008**, *130*, 10515–10517.
34. Scepaniak, J. J.; Young, J. A.; Bontchev, R. P.; Smith, J. M., Formation of Ammonia from an Iron Nitrido Complex. *Angew. Chem. Int. Ed.* **2009**, *48*, 3158-3160.

35. Scepaniak, J. J.; Vogel, C. S.; Khusniyarov, M. M.; Heinemann, F. W.; Meyer, K.; Smith, J. M., Synthesis, Structure, and Reactivity of an Iron(V) Nitride. *Science* **2011**, *331*, 1049-1052.
36. Searles, K.; Fortier, S.; Khusniyarov, M. M.; Carroll, P. J.; Sutter, J.; Meyer, K.; Mindiola, D. J.; Caulton, K. G., A cis-Divacant Octahedral and Mononuclear Iron(IV) Imide. *Angew. Chem. Int. Ed.* **2014**, *53*, 14139-14143.
37. Hennessy, E. T.; Liu, R. Y.; Iovan, D. A.; Duncan, R. A.; Betley, T. A., Iron-mediated intermolecular N-group transfer chemistry with olefinic substrates. *Chem. Sci.* **2014**, *5*, 1526-1532.
38. Iovan, D. A.; Betley, T. A., Characterization of Iron-Imido Species Relevant for N-Group Transfer Chemistry. *J. Am. Chem. Soc.* **2016**, *138*, 1983-1993.
39. Bellemin-Laponnaz, S.; Dagorne, S., Group 1 and 2 and Early Transition Metal Complexes Bearing N-Heterocyclic Carbene Ligands: Coordination Chemistry, Reactivity, and Applications. *Chem. Rev.* **2014**, *114*, 8747-8774.
40. Santini, C.; Marinelli, M.; Pellei, M., Boron-Centered Scorpionate-Type NHC-Based Ligands and Their Metal Complexes. *Eur. J. Inorg. Chem.* **2016**, *2016*, 2312-2331.
41. Trofimenko, S., *Scorpionates: Polypyrazolylborate Ligands and Their Coordination Chemistry*. Imperial College Press: London, 1999.
42. Pettinari, C., *Scorpionates II: Chelating Borate Ligands*. Imperial College Press: London, 2008.
43. Calabrese, J. C.; Trofimenko, S.; Thompson, J. S., A New Class of Polypyrazolylborate Ligands. *J. Chem. Soc., Chem. Commun.* **1986**, 1122-1123.
44. Trofimenko, S.; Calabrese, J. C.; Thompson, J. S., Novel polypyrazolylborate ligands: coordination control through 3-substituents of the pyrazole ring. *Inorg. Chem.* **1987**, *26*, 1507-1514.
45. Reinaud, O. M.; Rheingold, A. L.; Theopold, K. H., [Hydrotris(3-isopropyl-5-methylpyrazolyl)borato]iodocobalt(II): Unusual Purification by "Inverse Recrystallization". *Inorg. Chem.* **1994**, *33*, 2306-2308.
46. Shapiro, I. R.; Jenkins, D. M.; Thomas, J. C.; Day, M. W.; Peters, J. C., A homoleptic phosphine adduct of Tl(I). *Chem. Commun.* **2001**, 2152-2153.
47. Jenkins, D. M.; Di Bilio, A. J.; Allen, M. J.; Betley, T. A.; Peters, J. C., Elucidation of a Low Spin Cobalt(II) System in a Distorted Tetrahedral Geometry. *J. Am. Chem. Soc.* **2002**, *124*, 15336-15350.
48. Wasbotten, I. H.; Ghosh, A., Spin-State Energetics and Spin-Crossover Behavior of Pseudotetrahedral Cobalt(III)−Imido Complexes. The Role of the Tripodal Supporting Ligand. *Inorg. Chem.* **2007**, *46*, 7890-7898.
49. Lin, H.-J.; Siretanu, D.; Dickie, D. A.; Subedi, D.; Scepaniak, J. J.; Mitcov, D.; Clérac, R.; Smith, J. M., Steric and Electronic Control of the Spin State in Three-Fold Symmetric, Four-Coordinate Iron(II) Complexes. *J. Am. Chem. Soc.* **2014**, *136*, 13326-13332.
50. Creutz, S. E.; Peters, J. C., Spin-State Tuning at Pseudo-tetrahedral d^6 Ions: Spin Crossover in $[BP_3]Fe^{II}$–X Complexes. *Inorg. Chem.* **2016**, *55*, 3894-3906.
51. Jenkins, D. M.; Peters, J. C., Spin-State Tuning at Pseudotetrahedral d^7 Ions: Examining the Structural and Magnetic Phenomena of Four-Coordinate $[BP_3]Co^{II}$–X Systems. *J. Am. Chem. Soc.* **2005**, *127*, 7148-7165.
52. Tangen, E.; Conradie, J.; Ghosh, A., Bonding in Low-Coordinate Environments: Electronic Structure of Pseudotetrahedral Iron−Imido Complexes. *J. Chem. Theory Comp.* **2007**, *3*, 448-457.

53. Zolnhofer, E. M.; Käß, M.; Khusniyarov, M. M.; Heinemann, F. W.; Maron, L.; van Gastel, M.; Bill, E.; Meyer, K., An Intermediate Cobalt(IV) Nitrido Complex and its *N*-Migratory Insertion Product. *J. Am. Chem. Soc.* **2014**, *136*, 15072-15078.
54. Travieso-Puente, R.; Broekman, J. O. P.; Chang, M.-C.; Demeshko, S.; Meyer, F.; Otten, E., Spin-Crossover in a Pseudo-tetrahedral Bis(formazanate) Iron Complex. *J. Am. Chem. Soc.* **2016**, *138*, 5503-5506.
55. Scepaniak, J. J.; Bontchev, R. P.; Johnson, D. L.; Smith, J. M., Snapshots of Complete Nitrogen Atom Transfer from an Iron(IV) Nitrido Complex. *Angew. Chem. Int. Ed.* **2011**, *50*, 6630-6633.
56. Scepaniak, J. J.; Margarit, C. G.; Harvey, J. N.; Smith, J. M., Nitrogen Atom Transfer from Iron(IV) Nitrido Complexes: A Dual-Nature Transition State for Atom Transfer. *Inorg. Chem.* **2011**, *50*, 9508-9517.
57. Lee, W.-T.; Juarez, R. A.; Scepaniak, J. J.; Muñoz, S. B.; Dickie, D. A.; Wang, H.; Smith, J. M., Reaction of an Iron(IV) Nitrido Complex with Cyclohexadienes: Cycloaddition and Hydrogen-Atom Abstraction. *Inorg. Chem.* **2014**, *53*, 8425-8430.
58. Muñoz III, S. B.; Lee, W.-T.; Dickie, D. A.; Scepaniak, J. J.; Subedi, D.; Pink, M.; Johnson, M. D.; Smith, J. M., Styrene Aziridination by Iron(IV) Nitrides. *Angew. Chem. Int. Ed.* **2015**, *54*, 10600-10603.
59. Ding, M.; Rouzières, M.; Losovyj, Y.; Pink, M.; Clérac, R.; Smith, J. M., Partial Nitrogen Atom Transfer: A New Synthetic Tool to Design Single-Molecule Magnets. *Inorg. Chem.* **2015**, *54*, 9075-9080.
60. The two *e* orbitals do mix, unless the symmetry is D_{3h}, which is not the case for these ideally C_{3v} symmetry complexes. There is thus an indirect effect of the unoccupied $e_{(b)}$ orbitals on the filled $e_{(a)}$ orbitals.
61. McGarvey, B. R.; Telser, J., Simple Ligand-Field Theory of d^4 and d^6 Transition Metal Complexes with a C_3 Symmetry Axis. *Inorg. Chem.* **2012**, *51*, 6000-6010.
62. Zadrozny, J. M.; Niklas, J.; Poluektov, O. G.; Freedman, D. E., Millisecond Coherence Time in a Tunable Molecular Electronic Spin Qubit. *ACS Central Science* **2015**, *1*, 488-492.
63. Jeon, I.-R.; Park, J. G.; Haney, C. R.; Harris, T. D., Spin crossover iron(II) complexes as PARACEST MRI thermometers. *Chem. Sci.* **2014**, *5*, 2461-2465.
64. TIMEN = ***t***ris[2-(3-aryl-***im***idazol-2-ylidene)***e***thyl]ami***n***e; specific aryl substituents are indicated as TIMEN^{Ar}, where Ar = xylyl (Xyl), mesityl (Mes).
65. Krzystek, J.; Ozarowski, A.; Telser, J., Multi-frequency, high-field EPR as a powerful tool to accurately determine zero-field splitting in high-spin transition metal coordination complexes. *Coord. Chem. Rev.* **2006**, *250*, 2308-2324.
66. Telser, J.; Krzystek, J.; Ozarowski, A., High-frequency and high-field electron paramagnetic resonance (HFEPR): a new spectroscopic tool for bioinorganic chemistry. *JBIC Journal of Biological Inorganic Chemistry* **2014**, *19*, 297-318.
67. Nehrkorn, J.; Telser, J.; Holldack, K.; Stoll, S.; Schnegg, A., Simulating Frequency-Domain Electron Paramagnetic Resonance: Bridging the Gap between Experiment and Magnetic Parameters for High-Spin Transition-Metal Ion Complexes. *The Journal of Physical Chemistry B* **2015**, *119*, 13816-13824.
68. Nehrkorn, J.; Martins, B. M.; Holldack, K.; Stoll, S.; Dobbek, H.; Bittl, R.; Schnegg, A., Zero-field splittings in metHb and metMb with aquo and fluoro ligands: a FD-FT THz-EPR study. *Molecular Physics* **2013**, *111*, 2696-2707.

69. Schnegg, A.; Behrends, J.; Lips, K.; Bittl, R.; Holldack, K., Frequency domain Fourier transform THz-EPR on single molecule magnets using coherent synchrotron radiation. *Phys. Chem. Chem. Phys.* **2009**, *11*, 6820-6825.
70. Shaik, S.; Kumar, D.; de Visser, S. P.; Altun, A.; Thiel, W., Theoretical perspective on the structure and mechanism of cytochrome P450 enzymes. *Chem. Rev.* **2005**, *105*, 2279-2328.
71. Meunier, B.; de Visser, S. P.; Shaik, S., Mechanism of oxidation reactions catalyzed by cytochrome P450 enzymes. *Chem. Rev.* **2004**, *104*, 3947-3980.
72. Usharani, D.; Janardanan, D.; Li, C.; Shaik, S., A Theory for Bioinorganic Chemical Reactivity of Oxometal Complexes and Analogous Oxidants: The Exchange and Orbital-Selection Rules. *Acc. Chem. Res.* **2013**, *46*, 471–482.
73. Puri, M.; Que, L., Jr., Toward the Synthesis of More Reactive $S = 2$ Non-Heme Oxoiron(IV) Complexes. *Acc. Chem. Res.* **2015**, *48*, 2443-2452.
74. Que, L., Jr., The Road to Non-Heme Oxoferryls and Beyond. *Acc. Chem. Res.* **2007**, *40*, 493-500.
75. Tang, H.; Guan, J.; Liu, H.; Huang, X., Comparative Insight into Electronic Properties and Reactivities toward C–H Bond Activation by Iron(IV)–Nitrido, Iron(IV)–Oxo, and Iron(IV)–Sulfido Complexes: A Theoretical Investigation. *Inorg. Chem.* **2013**, *52*, 2684-2696.
76. Vardhaman, A. K.; Barman, P.; Kumar, S.; Sastri, C. V.; Kumar, D.; De Visser, S. P., Comparison of the Reactivity of Nonheme Iron(IV)–Oxo versus Iron(IV)–Imido Complexes: Which is the Better Oxidant? *Angew. Chem. Int. Ed.* **2013**, *52*, 12288-12292.
77. Geng, C.; Ye, S.; Neese, F., Does a higher metal oxidation state necessarily imply higher reactivity toward H-atom transfer? A computational study of C–H bond oxidation by high-valent iron-oxo and -nitrido complexes. *Dalton Trans.* **2014**, *43*, 6079-6086.
78. Cohen, S.; Ma, J.; Butenschön, H.; Herber, R. H., Metal atom dynamics in four triferrocenylmethane derivatives and the crystal structure of Fc_3COH. *Dalton Trans.* **2009**, 6606-6609.
79. Herber, R. H., Structure, Bonding, and the Mössbauer Lattice Temperature. In *Chemical Mössbauer Spectroscopy*, Herber, R. H., Ed. Plenum Press: New York, 1984; pp 199-216.
80. Herber, R. H.; Nowik, I.; Cohen, S., Metal atom dynamics in organometallics: Resolving the dichotomy between Mössbauer and X-ray derived values. *J. Phys. Conf. Ser.* **2010**, *217*, 012145.
81. Herber, R. H.; Nowik, I., Metal Atom Dynamics of Organotin Compounds. *Phosphorus, Sulfur, and Silicon and the Related Elements* **2011**, *186*, 1336-1340.
82. Herber, R. H., Iron and tin atom dynamics and hyperfine interactions of two structurally related half-sandwich complexes bearing a distannyl moiety. *J. Organomet. Chem.* **2012**, *717*, 41-44.
83. Herber, R. H., Lattice dynamics of the two distinct Fe atoms in $Ar(dppe)FeGaFe(CO)_4$ (Ar = Cp and Cp^*). *J. Organomet. Chem.* **2013**, *745–746*, 284-287.
84. Harder, S.; Naglav, D.; Schwerdtfeger, P.; Nowik, I.; Herber, R. H., Metal Atom Dynamics in Superbulky Metallocenes: A Comparison of $(Cp^{BIG})_2Sn$ and $(Cp^{BIG})_2Eu$. *Inorg. Chem.* **2014**, *53*, 2188-2194.
85. Bogoslavsky, B.; Nowik, I.; Herber, R. H., Hyperfine Interactions and Metal Atom Dynamics in a Number of Stannyl Phosphide Compounds and the Detailed Crystal Structure of Triphenyltin Chloride Revisited. *Eur. J. Inorg. Chem.* **2016**, *2016*, 1619-1624.
86. Herber, R. H.; Felner, I.; Nowik, I., Lattice dynamics, phase transitions and spin relaxation in $[Fe(C_5H_5)_2]PF_6$. *Hyperfine Interactions* **2016**, *237*, 100.

87. Prisecaru, I. *WMOSS4 Mössbauer Spectral Analysis Software*, version F, released on Feb. 27 2013; 2009-2016.
88. Gütlich, P.; Bill, E.; Trautwein, A. X., *Mössbauer Spectroscopy and Transition Metal Chemistry: Fundamentals and Applications*. Springer-Verlag Berlin Heidelberg: Heidelberg, Germany, 2011; p XV, 569.
89. Hassan, A. K.; Pardi, L. A.; Krzystek, J.; Sienkiewicz, A.; Goy, P.; Rohrer, M.; Brunel, L.-C., Ultrawide band multifrequency high-field EMR technique: a methodology for increasing spectroscopic information. *J. Magn. Reson.* **2000**, *142*, 300-312.
90. Zvyagin, S. A.; Krzystek, J.; van Loosdrecht, P. H. M.; Dhalenne, G.; Revcolevschi, A., High-field ESR study of the dimerized-incommensurate phase transition in the spin-Peierls compound $CuGeO_3$. *Physica B* **2004**, *346-347*, 1-5.
91. Stoll, S.; Schweiger, A., EasySpin, a comprehensive software package for spectral simulation and analysis in EPR. *J. Magn. Reson.* **2006**, *178*, 42-55.
92. Bain, G. A.; Berry, J. F., Diamagnetic Corrections and Pascal's Constants. *J. Chem. Educ.* **2008**, *85*, 532-536.
93. Bendix, J., Ligfield. In *Comprehensive Coordination Chemistry II, Volume 2: Fundamentals: Physical Methods, Theoretical Analysis, and Case Studies*, Lever, A. B. P., Ed. Elsevier: Amsterdam, 2003; Vol. 2, pp 673-676.
94. Brorson, M.; Schäffer, C. E., Orthonormal interelectronic repulsion operators in the parametrical d^q model. Application of the model to gaseous ions. *Inorg. Chem.* **1988**, *27*, 2522-2530.
95. Bendix, J.; Brorson, M.; Schäffer, C. E., Accurate empirical spin orbit coupling parameters ζ_{nd} for gaseous nd^q transition metal ions. The parametrical multiplet term model. *Inorg. Chem.* **1993**, *32*, 2838-2849.
96. Frisch, M. J. T., G. W.; Schlegel, H. B.; Scuseria, G. E.; Robb, M. A.; Cheeseman, J. R.; Scalmani, G.; Barone, V.; Mennucci, B.; Petersson, G. A.; Nakatsuji, H.; Caricato, M.; Li, X.; Hratchian, H. P.; Izmaylov, A. F.; Bloino, J.; Zheng, G.; Sonnenberg, J. L.; Hada, M.; Ehara, M.; Toyota, K.; Fukuda, R.; Hasegawa, J.; Ishida, M.; Nakajima, T.; Honda, Y.; Kitao, O.; Nakai, H.; Vreven, T.; Montgomery, J. A., Jr.; Peralta, J. E.; Ogliaro, F.; Bearpark, M.; Heyd, J. J.; Brothers, E.; Kudin, K. N.; Staroverov, V. N.; Kobayashi, R.; Normand, J.; Raghavachari, K.; Rendell, A.; Burant, J. C.; Iyengar, S. S.; Tomasi, J.; Cossi, M.; Rega, N.; Millam, J. M.; Klene, M.; Knox, J. E.; Cross, J. B.; Bakken, V.; Adamo, C.; Jaramillo, J.; Gomperts, R.; Stratmann, R. E.; Yazyev, O.; Austin, A. J.; Cammi, R.; Pomelli, C.; Ochterski, J. W.; Martin, R. L.; Morokuma, K.; Zakrzewski, V. G.; Voth, G. A.; Salvador, P.; Dannenberg, J. J.; Dapprich, S.; Daniels, A. D.; Farkas, Ö.; Foresman, J. B.; Ortiz, J. V.; Cioslowski, J.; Fox, D. J. Gaussian, Inc., Wallingford CT, 2009. *Gaussian 09, Revision D.01*, Revision D.01; Wallingford, CT, 2009.
97. Lee, C.; Yang, W.; Parr, R. G., Development of the Colle-Salvetti correlation-energy formula into a functional of the electron density. *Phys. Rev. B* **1988**, *37*, 785-789.
98. Becke, A. D., Density-functional Thermochemistry. III. The Role of Exact Exchange. *J. Chem. Phys.* **1993**, *98*, 5648-5652.
99. Stephens, P. J.; Devlin, F. J.; Chabalowski, C. F.; Frisch, M. J., Ab Initio Calculation of Vibrational Absorption and Circular Dichroism Spectra Using Density Functional Force Fields. *J. Phys. Chem.* **1994**, *98*, 11623-11627.
100. Vosko, S. H.; Wilk, L.; Nusair, M., Accurate spin-dependent electron liquid correlation energies for local spin density calculations: a critical analysis. *Can. J. Phys.* **1980**, *58*, 1200-1211.

101. Krishnan, R.; Binkley, J. S.; Seeger, R.; Pople, J. A., Self-consistent molecular orbital methods. XX. A basis set for correlated wave functions. *J. Chem. Phys.* **1980**, *72*, 650-654.
102. McLean, A. D.; Chandler, G. S., Contracted Gaussian basis sets for molecular calculations. I. Second row atoms, Z=11–18. *J. Chem. Phys.* **1980**, *72*, 5639-5648.
103. Wachters, A. J. H., Gaussian Basis Set for Molecular Wavefunctions Containing Third-Row Atoms. *J. Chem. Phys.* **1970**, *52*, 1033-1036.
104. Bachler, V.; Olbrich, G.; Neese, F.; Wieghardt, K., Theoretical Evidence for the Singlet Diradical Character of Square Planar Nickel Complexes Containing Two o-Semiquinonato Type Ligands. *Inorg. Chem.* **2002**, *41*, 4179-4193.
105. Yamaguchi, K.; Tsunekawa, T.; Toyoda, Y.; Fueno, T., Ab initio molecular orbital calculations of effective exchange integrals between transition metal ions. *Chem. Phys. Lett.* **1988**, *143*, 371-376.
106. Neese, F., Importance of Direct Spin−Spin Coupling and Spin-Flip Excitations for the Zero-Field Splittings of Transition Metal Complexes: A Case Study. *J. Am. Chem. Soc.* **2006**, *128*, 10213-10222.
107. Neese, F., Prediction of electron paramagnetic resonance g values using coupled perturbed Hartree–Fock and Kohn–Sham theory. *J. Chem. Phys.* **2001**, *115*, 11080-11096.
108. Sandhoefer, B.; Neese, F., One-electron contributions to the g-tensor for second-order Douglas–Kroll–Hess theory. *J. Chem. Phys.* **2012**, *137*, 094102.
109. Neese, F. *ORCA - an ab initio, Density Functional and Semiempirical Program Package*, 3.0.3; Max Planck Institut für Chemische Energiekonversion: Mülheim an der Ruhr, Germany, 2014.
110. Schäfer, A.; Horn, H.; Ahlrichs, R., Fully optimized contracted Gaussian basis sets for atoms Li to Kr. *J. Chem. Phys.* **1992**, *97*, 2571-2577.
111. Neese, F., Calculation of the zero-field splitting tensor on the basis of hybrid density functional and Hartree-Fock theory. *J. Chem. Phys.* **2007**, *127*, 164112.
112. Römelt, M.; Ye, S.; Neese, F., Calibration of Modern Density Functional Theory Methods for the Prediction of ^{57}Fe Mössbauer Isomer Shifts: Meta-GGA and Double-Hybrid Functionals. *Inorg. Chem.* **2009**, *48*, 784-785.
113. Tao, J.; Perdew, J. P.; Staroverov, V. N.; Scuseria, G. E., Climbing the Density Functional Ladder: Nonempirical Meta-Generalized Gradient Approximation Designed for Molecules and Solids. *Phys. Rev. Lett.* **2003**, *91*, 146401.
114. Klamt, A.; Schuurmann, G., COSMO: a new approach to dielectric screening in solvents with explicit expressions for the screening energy and its gradient. *J. Chem. Soc., Perkin Trans. 2* **1993**, 799-805.
115. Sinnecker, S.; Slep, L. D.; Bill, E.; Neese, F., Performance of Nonrelativistic and Quasi-Relativistic Hybrid DFT for the Prediction of Electric and Magnetic Hyperfine Parameters in ^{57}Fe Mössbauer Spectra. *Inorg. Chem.* **2005**, *44*, 2245-2254.
116. Duboc, C.; Ganyushin, D.; Sivalingam, K.; Collomb, M.-N.; Neese, F., Systematic Theoretical Study of the Zero-Field Splitting in Coordination Complexes of Mn(III). Density Functional Theory versus Multireference Wave Function Approaches. *J. Phys. Chem. A* **2010**, *114*, 10750-10758.
117. Zein, S.; Neese, F., Ab Initio and Coupled-Perturbed Density Functional Theory Estimation of Zero-Field Splittings in Mn^{II} Transition Metal Complexes. *J. Phys. Chem. A* **2008**, *112*, 7976–7983.

118. Romain, S.; Duboc, C.; Neese, F.; Rivière, E.; Hanton, L. R.; Blackman, A. G.; Philouze, C.; Leprêtre, J.-C.; Deronzier, A.; Collomb, M.-N., An Unusual Stable Mononuclear Mn^{III} Bis-terpyridine Complex Exhibiting Jahn–Teller Compression: Electrochemical Synthesis, Physical Characterisation and Theoretical Study. *Chem. Eur. J.* **2009**, *15*, 980-988.
119. Pipek, J.; Mezey, P. G., A fast intrinsic localization procedure applicable for ab initio and semiempirical linear combination of atomic orbital wave functions. *J. Chem. Phys.* **1989**, *90*, 4916-4926.
120. Bader, R. F. W., *Atoms in Molecules: A Quantum Theory*. Clarendon Press: Oxford, UK, 1994.
121. Biegler–König, F.; Schönbohm, J.; Bayles, D., AIM2000. *Journal of Computational Chemistry* **2001**, *22*, 545-559.
122. Andrienko, G. A. *Chemcraft*, 1.8 (build 405); 2015.
123. CSD codes CEKBOK and CEKBUQ, respectively for R = H, 3,5-Me_2.
124. Eisenhardt, R. J.; Rudd, P. A.; Planas, N.; Boyce, D. W.; Carlson, R. K.; Tolman, W. B.; Bill, E.; Gagliardi, L.; Lu, C. C., Pushing the Limits of Delta Bonding in Metal−Chromium Complexes with Redox Changes and Metal Swapping. *Inorg. Chem.* **2015**, 7579-7592.
125. Rudd, P. A.; Liu, S.; Planas, N.; Bill, E.; Gagliardi, L.; Lu, C. C., Multiple Metal–Metal Bonds in Iron–Chromium Complexes. *Angew. Chem. Int. Ed.* **2013**, *52*, 4449-4452.
126. Scepaniak, J. J.; Harris, T. D.; Vogel, C. S.; Sutter, J.; Meyer, K.; Smith, J. M., Spin Crossover in a Four-Coordinate Iron(II) Complex. *J. Am. Chem. Soc.* **2011**, *133*, 3824-3827.
127. Klinker, E. J.; Jackson, T. A.; Jensen, M. P.; Stubna, A.; Juhász, G.; Bominaar, E. L.; Münck, E.; Que, L., Jr., A Tosylimido Analogue of a Nonheme Oxoiron(IV) Complex. *Angew. Chem. Int. Ed.* **2006**, *45*, 7394-7397.
128. Cutsail III, G. E.; Telser, J.; Hoffman, B. M., Advanced paramagnetic resonance spectroscopies of iron–sulfur proteins: Electron nuclear double resonance (ENDOR) and electron spin echo envelope modulation (ESEEM). *Biochimica et Biophysica Acta (BBA) - Molecular Cell Research* **2015**, *1853*, 1370-1394.
129. Boča, R., Zero-field splitting in metal complexes. *Coord. Chem. Rev.* **2004**, *248*, 757-815.
130. Boča, R., *Theoretical Foundations of Molecular Magnetism*. Elsevier: Amsterdam, 1999.
131. Boča, R., Magnetic Parameters and Magnetic Functions in Mononuclear Complexes Beyond the Spin-Hamiltonian Formalism. *Structure and Bonding* **2006**, *117*, 1-264.
132. Krzystek, J.; Telser, J., Measuring giant anisotropy in paramagnetic transition metal complexes with relevance to single-ion magnetism. *Dalton Transactions* **2016**, *45*, 16751-16763.
133. Krzystek, J.; England, J.; Ray, K.; Ozarowski, A.; Smirnov, D.; Que, L., Jr.; Telser, J., Determination by High-Frequency and -Field EPR of Zero-Field Splitting in Iron(IV) Oxo Complexes: Implications for Intermediates in Nonheme Iron Enzymes. *Inorg. Chem.* **2008**, *47*, 3483-3485.
134. Since only one HFEPR transition is observed, disregarding the splitting at higher fields due to *g* anisotropy, we lack the ability to compare relative intensities, which would allow determination of the sign of *D* in these complexes.
135. Bucinsky, L.; Rohde, G. T.; Que, L., Jr.; Ozarowski, A.; Krzystek, J.; Breza, M.; Telser, J., HFEPR and Computational Studies on the Electronic Structure of a High-Spin Oxidoiron(IV) Complex in Solution. *Inorg. Chem.* **2016**, *55*, 3933-3945.

136. For example, the three C(carbene)-Fe-C(carbene) angles in **4** (CSD: MOBNUN) are nearly equal: ∠C1-Fe-C13 = 89.10°, ∠C1-Fe-C13 = 89.35°, and ∠C13-Fe-C25 = 89.37°; see Table S6 for further information.
137. Schäffer, C. E., A Perturbation Representation of Weak Covalent Bonding. *Struct. Bonding* **1968**, *5*, 68-95.
138. Figgis, B. N.; Hitchman, M. A., *Ligand Field Theory and its Applications*. Wiley-VCH: New York, 2000.
139. Srnec, M.; Wong, S. D.; England, J.; Que, L., Jr.; Solomon, E. I., π-Frontier molecular orbitals in *S* = 2 ferryl species and elucidation of their contributions to reactivity. *Proc. Natl. Acad. Sci. USA* **2012**, *109*, 14326-14331.
140. Meyer, K.; Bendix, J.; Bill, E.; Weyhermüller, T.; Wieghardt, K., Molecular and Electronic Structure of Nitridochromium(V) Complexes with Macrocyclic Amine Ligands. *Inorg. Chem.* **1998**, *37*, 5180-5188.
141. Meyer, K.; Bendix, J.; Metzler-Nolte, N.; Weyhermüller, T.; Wieghardt, K., Nitridomanganese(V) and -(VI) Complexes Containing Macrocyclic Amine Ligands. *J. Am. Chem. Soc.* **1998**, *120*, 7260-7270.
142. Forshaw, A. P.; Smith, J. M.; Ozarowski, A.; Krzystek, J.; Smirnov, D.; Zvyagin, S. A.; Harris, T. D.; Karunadasa, H. I.; Zadrozny, J. M.; Schnegg, A.; Holldack, K.; Jackson, T. A.; Alamiri, A.; Barnes, D. M.; Telser, J., Low-Spin Hexacoordinate Mn(III): Synthesis and Spectroscopic Investigation of Homoleptic Tris(pyrazolyl)borate and Tris(carbene)borate Complexes. *Inorg. Chem.* **2013**, *52*, 144–159.
143. Nieto, I.; Bontchev, R. P.; Ozarowski, A.; Smirnov, D.; Krzystek, J.; Telser, J.; Smith, J. M., Synthesis and spectroscopic investigations of four-coordinate nickel complexes supported by a strongly donating scorpionate ligand. *Inorg. Chim. Acta* **2009**, *362*, 4449-4460.
144. In this complex, the *z* axis is defined along the Fe-N_{imido} bond with the equatorial vacancy defining the *x* axis. In contrast to the trigonal complexes, there is thus a significant energy difference between the d_{yz} and d_{xz} orbitals (both π*), with the latter much lower in energy and thus filled. The approximately non-bonding d_{xy} orbital is also filled, while the d_{z^2} and $d_{x^2-y^2}$ orbitals (both σ*) are much higher in energy and unoccupied, to give overall the $d_{xy}^{\ 2}d_{xz}^{\ 2}d_{yz}^{\ 0}d_{z^2}^{\ 0}d_{x^2-y^2}^{\ 0}$ ground state, singlet spin electronic configuration.
145. The average values for **1** and **1·MeCN** are essentially identical; see Table S6, Supporting Information.
146. For simplicity, we use the notation **3** and **4** to refer solely to the cations of **3** and **4** as studied computationally, while these are the full ion-counterion complexes (i.e., Fe complex cation with the BPh_4^- counteranion) when studied experimentally by whatever technique.
147. Cutsail III, G. E.; Stein, B. W.; Subedi, D.; Smith, J. M.; Kirk, M. L.; Hoffman, B. M., EPR, ENDOR, and Electronic Structure Studies of the Jahn–Teller Distortion in an Fe^V Nitride. *J. Am. Chem. Soc.* **2014**, *136*, 12323-12336.
148. By contrast, the longer Fe-C dative bonds in the imido complexes imply shorter C-N and C-B bond lengths in the NHC rings and vice versa for nitridos.
149. Stavretis, S. E.; Atanasov, M.; Podlesnyak, A. A.; Hunter, S. C.; Neese, F.; Xue, Z.-L., Magnetic Transitions in Iron Porphyrin Halides by Inelastic Neutron Scattering and Ab Initio Studies of Zero-Field Splittings. *Inorg. Chem.* **2015**, *54*, 9790-9801.
150. Havenith, R. W. A.; Taylor, P. R.; Angeli, C.; Cimiraglia, R.; Ruud, K., Calibration of the n-electron valence state perturbation theory approach. *J. Chem. Phys.* **2004**, *120*, 4619-4625.

151. Schapiro, I.; Sivalingam, K.; Neese, F., Assessment of n-Electron Valence State Perturbation Theory for Vertical Excitation Energies. *J. Chem. Theory Comp.* **2013**, *9*, 3567-3580.
152. Vancoillie, S.; Delcey, M. G.; Lindh, R.; Vysotskiy, V.; Malmqvist, P.-Å.; Veryazov, V., Parallelization of a multiconfigurational perturbation theory. *J. Comp. Chem.* **2013**, *34*, 1937-1948.
153. Angeli, C.; Cimiraglia, R.; Evangelisti, S.; Leininger, T.; Malrieu, J.-P., Introduction of n-electron valence states for multireference perturbation theory. *J. Chem. Phys.* **2001**, *114*, 10252-10264.
154. Angeli, C.; Cimiraglia, R.; Malrieu, J.-P., N-electron valence state perturbation theory: a fast implementation of the strongly contracted variant. *Chem. Phys. Lett.* **2001**, *350*, 297-305.
155. Angeli, C.; Evangelisti, S.; Cimiraglia, R.; Maynau, D., A novel perturbation-based complete active space–self-consistent-field algorithm: Application to the direct calculation of localized orbitals. *J. Chem. Phys.* **2002**, *117*, 10525-10533.
156. Werncke, C. G.; Suturina, E.; Bunting, P. C.; Vendier, L.; Long, J. R.; Atanasov, M.; Neese, F.; Sabo-Etienne, S.; Bontemps, S., Homoleptic Two-Coordinate Silylamido Complexes of Chromium(I), Manganese(I), and Cobalt(I). *Chem. Eur. J.* **2016**, *22*, 1668-1674.
157. Suturina, E. A.; Maganas, D.; Bill, E.; Atanasov, M.; Neese, F., Magneto-Structural Correlations in a Series of Pseudotetrahedral $[Co^{II}(XR)_4]^{2-}$ Single Molecule Magnets: An ab Initio Ligand Field Study. *Inorg. Chem.* **2015**, *54*, 9948-9961.
158. Schweinfurth, D.; Sommer, M. G.; Atanasov, M.; Demeshko, S.; Hohloch, S.; Meyer, F.; Neese, F.; Sarkar, B., The Ligand Field of the Azido Ligand: Insights into Bonding Parameters and Magnetic Anisotropy in a Co(II)–Azido Complex. *J. Am. Chem. Soc.* **2015**, *137*, 1993-2005.
159. Rechkemmer, Y.; Breitgoff, F. D.; van der Meer, M.; Atanasov, M.; Hakl, M.; Orlita, M.; Neugebauer, P.; Neese, F.; Sarkar, B.; van Slageren, J., A four-coordinate cobalt(II) single-ion magnet with coercivity and a very high energy barrier. *Nature Comm.* **2016**, *7*, 10467.
160. The CASSCF(10,7) calculation yields g_x and g_y values close to 2.01 and the g_z value is 2.08.
161. CASSCF single reference ansatz has been employed to allow evaluation of each AO's contribution via localization of the active space orbitals.
162. Natural bonding orbital is a general term we apply to orbitals generated from the CASSCF calculations, which individually could be bonding, anti-bonding, or non-bonding in character.
163. Fukuzumi, S.; Ohkubo, K.; Lee, Y.-M.; Nam, W., Lewis Acid Coupled Electron Transfer of Metal–Oxygen Intermediates. *Chemistry – A European Journal* **2015**, *21*, 17548-17559.
164. Nam, W.; Lee, Y.-M.; Fukuzumi, S., Tuning Reactivity and Mechanism in Oxidation Reactions by Mononuclear Nonheme Iron(IV)-Oxo Complexes. *Acc. Chem. Res.* **2014**, *47*, 1146-1154.
165. Park, J.; Morimoto, Y.; Lee, Y.-M.; Nam, W.; Fukuzumi, S., Unified View of Oxidative C–H Bond Cleavage and Sulfoxidation by a Nonheme Iron(IV)–Oxo Complex via Lewis Acid-Promoted Electron Transfer. *Inorg. Chem.* **2014**, *53*, 3618-3628.

For Table of Contents Only

Experimentally-correlated electronic structure calculations of three-fold symmetric iron(IV) imido and nitrido complexes at various levels of theory reveal that spin state of the complex is determined by the relative energy of a single orbital, whose energy is tuned by the σ-donor ability of the multiply bonded ligand. Symmetry breaking / restoring of the orbitally degenerate ground state of the imido complexes is also explored by these techniques.